UCLouvain

École polytechnique de Louvain

Stochastic geometric analysis of RIS aided wireless networks

Author: **Nicolas Rorive**
Supervisors: **Prof. Claude Oestges, Prof. Luc Vandendorpe**
Readers: **Prof. Jérôme Louveaux, Charles Wiame**
Academic year 2021–2022
Master [120] in Electrical Engineering

Acknowledgements

The achievement of this master thesis has been possible with the help and support of several people that I would like to thank:

First, I would like to thank Prof. Claude Oestges and Prof. Luc Vandendorpe for their availability, expertise and suggestions throughout the completion of this master thesis.

I would also like to thank Charles Wiame for his continuous help and meaningful feedback.

In addition, I would like to thank Simon Demey and the Ph.D students from the electrical engineering department at UCLouvain who have helped at some points during this academic year.

Then, I would like to acknowledge Prof. Jérôme Louveaux who agreed to read this master thesis.

Finally, I must express my gratitude to my family and my loved ones for their unlimited support.

Abstract

This master thesis aims at investigating the improvement of performance brought by the use of reconfigurable impedance surfaces (RIS) in wireless networks using a stochastic geometry approach. To this point, different situations are analysed where the non line-of-sight link using the RIS can be used together with the line-of-sight link. The links are subject to path loss and Nakagami-m distributed small-scale fading. First, the possibility of using multiple RIS together is studied. Then, cases where the links can be blocked by obstacles are modelled and different association rules are compared. For both schemes, the metric of performance will be the coverage probability.

Ce travail de fin d'études a pour objet l'analyse de l'amélioration de performance qu'apporterait l'utilisation de surfaces d'impédance reconfigurable (RIS) dans des réseaux sans-fil en utilisant l'approche de la géométrie stochastique. A cette fin, différentes situations sont analysées dans lesquelles le lien non ligne-de-vue utilisant les RIS peut être utilisé avec le lien ligne-de-vue. Les liens sont impactés par de l'atténuation de propagation et de l'évanouissement à petite échelle suivant une distribution de Nakagami-m. Tout d'abord, la possibilité d'utiliser plusieurs RIS en même temps est étudiée. Ensuite, des cas où les liens peuvent être bloqués par des obstacles sont modélisés et différentes règles d'association sont comparées. Pour les deux situations, la métrique de performance sera la probabilité de couverture.

List of Abbreviations

5G	5th generation
6G	6th generation
AWGN	Additive white gaussian noise
BPP	Binomial Point Process
BS	Base station
cdf	Cumulative distribution function
CF	Characteristic function
CLT	Central Limit Theorem
HPPP	Homogeneous Poisson Point Process
IPPP	Inhomogeneous Poisson Point Process
LoS	Line-of-Sight
MIMO	Multiple inputs multiple outputs
NLoS	Non Line-of-Sight
NOMA	Non-orthogonal multiple access
pdf	Probability distribution function
PGFL	Probability generating functional
pmf	Probability mass function
PP	Point process
PPP	Poisson Point Process
RCS	Radar-cross section
RIS	Reconfigurable impedance surfaces
RV	Random variable
SG	Stochastic Geometry
SINR	Signal to interference plus noise ratio
SNR	Signal to noise ratio

SRE Smart-Radio Environment

UAV Unmanned aerial vehicles

UE User end

Contents

1 Introduction **1**

2 State of the art **3**
2.1 Stochastic Geometry . . . 3
2.1.1 Point Process . . . 3
2.1.2 Types of Point Process . . . 4
2.1.3 Properties of the Poisson Point Process . . . 5
2.2 Probability fundamentals . . . 6
2.2.1 The central limit theorem . . . 6
2.2.2 The moment generating function and the characteristic function . . . 6
2.3 Reconfigurable Impedance Surfaces: Fundamentals . . . 7
2.3.1 Motivations . . . 7
2.3.2 Hardware architecture . . . 7
2.3.3 RIS-aided wireless networks . . . 8
2.3.4 Propagation model . . . 8
2.3.5 Further possible advancement . . . 10
2.4 Stochastic Geometry and Reconfigurable Impedance Surfaces . . . 10
2.4.1 Spatial diversity . . . 10
2.4.2 Impact of the RIS on interferences . . . 10
2.4.3 RIS to handle blockages . . . 11
2.4.4 Physical security layer . . . 12
2.4.5 Optimization of an RIS-aided network . . . 12
2.4.6 Advantages compared to other techniques . . . 12

3 On the joint use of multiple RIS in wireless networks **13**
3.1 Introduction . . . 13
3.2 System Model . . . 13
3.3 Coverage probability without interference . . . 15
3.3.1 One RIS with known location . . . 15
3.3.2 One RIS with random location . . . 17
3.3.3 Using a known number of RIS . . . 20
3.3.4 Using a random number of RIS . . . 22
3.4 Coverage Probability with Interference . . . 22
3.4.1 Channel Characterization . . . 23
3.4.2 The Characteristic Function of the Interfering Power . . . 24
3.5 Numerical results and analysis . . . 26
3.5.1 Improvement when using RIS compared to the LoS link . . . 27
3.5.2 Number of RIS to use . . . 28
3.5.3 Size of the zone with RIS . . . 29
3.6 Chapter Summary . . . 29

4 Association rules for RIS-aided wireless networks impaired by blockages **31**
4.1 Introduction . . . 31
4.2 System Model . . . 31
4.2.1 Geometric description of the network . . . 31
4.2.2 Association rules . . . 32
4.3 Coverage Probability . . . 33
4.3.1 Random fading gain . . . 33
4.3.2 The different types of link . . . 34
4.3.3 The distance between the UE and the BS . . . 35
4.3.4 Different Base Station . . . 36
4.3.5 The distance between the UE and the RIS . . . 37
4.3.6 Coverage Probability for Different Association Rules . . . 38
4.4 Validation and results . . . 39
4.4.1 Impact of blockages on the coverage probability . . . 39
4.4.2 Comparison between the density of RIS and the density of RIS . . . 41
4.5 Chapter summary . . . 42

5 Conclusion **45**
5.1 Summary of Contributions . . . 45
5.2 Further research directions . . . 45

A Central Limit Theorem Validation **48**

B Computation of the Characteristic Function of the Interfering Power **50**

C On the numerical evaluation of the Gil-Pelaez Inversion Law **52**

Bibliography **53**

Chapter 1

Introduction

Up until the 5th generation of wireless communications, the main way to cope with the growing requirements of data transmission was to consider the environment as not controllable and working only on the transmitters and receivers. For the 6G wireless communication, however, an emerging paradigms called "Smart-Radio Environment" [22] is studied. This paradigms aims at optimizing wireless communication by controlling the environment of propagation of the electromagnetic waves.
One of the devices used to apply the SRE paradigm is the RIS. This device will allow to control the angle of reflection of the electromagnetic wave in order to focus the beam to the receiver as shown in figure 1.1.

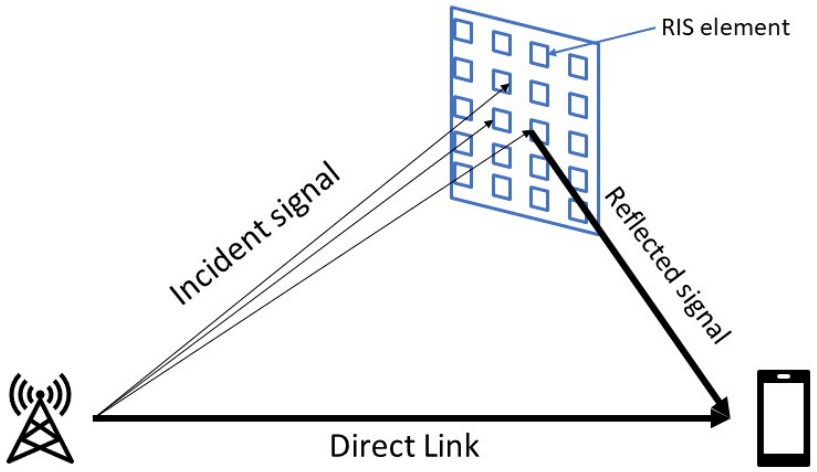

Figure 1.1: RIS reflection scheme

Such devices have already been prototyped, an example can be seen on figure 1.2. This RIS can be represented as an array of metasurfaces elements which will all reflect the incident wave in a way that can be configured. In chapter 2, an overview will be done on the fundamentals of the RIS and its modelling.
In a wireless network, the position of the UE, the BS and the RIS should be considered as random to model the mobility of the user and the fact that the transmission can take place in different environment. In order to quantify the performance of an RIS-aided wireless network, Monte-Carlo simulations could be used by sampling at each iteration different positions for the different elements of the network. The main drawbacks are that this approach can't give any closed form expression and the time of computation will increase with the number of element of the network. This is the reason why stochastic geometry will be used as this tool can theoretically model the random positions of the different elements of the network. The main advantage of stochastic geometry is that dense network (with a lot of

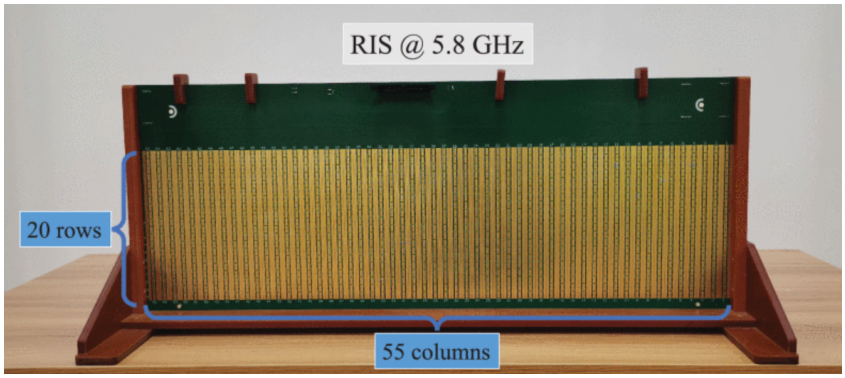

Figure 1.2: Example of build RIS in [21]

elements) can be modelled in an efficient way. Fundamentals of stochastic geometry are presented in chapter 2.
In chapter 3, a wireless network without blockage where both the UE and the BS have known position but the RIS are randomly located is modelled under interference. This chapter will focus on the joint use of multiple RIS at the same time to enhance the transmission. This chapter will rely on the assumption that several RIS can be tuned such as the signal coming from each RIS can be coherently added.
Finally, in chapter 4. A network with blockages and randomly located RIS and BS will be modelled. Here only on RIS at a time can be used, but it can be used jointly with line of sight link. The main focus of this chapter will be to compare different association rules as multiple BS are potentially available. The performance related to the number of RIS or their size will also be analysed.

Chapter 2

State of the art

This state of art will first present the basics of stochastic geometry and some probability fundamentals. Then an overview the fundamentals of the RIS and the path loss modelling of the RIS is made. The final section will consist in an overview of the literature over the stochastic geometry analysis of an RIS-aided wireless communication system.

2.1 Stochastic Geometry

Stochastic Geometry is a mathematical field which links geometry and probabilities theory to study random spatial patterns. As a wireless network can be modelled as set of nodes representing transmitters or receivers whose location in space is random, SG is a relevant tool to study wireless networks. SG has also been used in domains like medical image analysis, gas reactor design or even ecosystem dynamics. When using SG to analyse wireless networks, point processes are often used to model the transmitters or receiver nodes. By doing so, the evaluation of performance that is obtained is a spatial average which can highly differ from some particular cases. As the use of SG can lead to computationally heavy models, important assumptions must often be taken in order to simplify those models. Therefore the results of SG models should be compared with Monte-Carlo models to evaluate their relevancy. The advantages of SG compared to Monte-Carlo simulations is the ability to model large systems without increasing the complexity of the calculations.
In the following, the Point Process (PP) theory and the theorems that will be later used are developed. Most of the following is based on [1] and [5].

2.1.1 Point Process

Definition

PPs can be generally be defined on the d-dimensional Euclidean space $\mathbb{R}^d$. In this work, only PPs defined over $\mathbb{R}^2$ will be used to model the location of network nodes.
A spatial point process Φ is a random, finite or countably-infinite collection of points in the space $\mathbb{R}^d$. Any realization ϕ of a PP Φ can be considered as a subset $\phi = \{x_i\} \in \mathbb{R}^d$ or as a counting measure where $\psi(A)$ will give the number of points of Φ in a subset A of $\mathbb{R}^d$.

Characteristics

These characteristics of a Point Process will be later used and can be defined:

- **Density measure** $\lambda(x)$ (for $x \in \mathbb{R}^d$) can be linked to a counting measure $\psi(A)$ by the following equation:

$$\int_A \lambda(x)\mathrm{d}x \quad = \quad \mathbb{E}\left[\psi(A)\right] \tag{2.1}$$

A point process Φ for which $\lambda(x) = k, \forall x \in A$, is said to be homogeneous. Otherwise, Φ is said to be inhomogeneous.

Intensity measure $\Lambda(A)$ is linked to the density measure $\lambda(x)$ by:

$$\Lambda(A) = \int_A \lambda(x)\mathrm{d}x \tag{2.2}$$

- **Void probability** function v_Φ is function defined on A as:

$$v_\Phi(A) = \mathbb{P}(\psi(A) = 0) \tag{2.3}$$

- **Probability generating functional** for any real positive function f defined over $\mathbb{R}^d$, the PGFL of the PP with respect to this function is the expected value of the product of $f(x_i)$ for each $x_i \in \phi$.

$$\mathcal{P}_\phi(f) = \mathbb{E}\left[\prod_{x_i \in \phi} f(x_i)\right] \tag{2.4}$$

For a random variable $F = \sum_{x_i \in \phi} g(x_i)$, the PGFL can be used to compute its Laplace transform:

$$\begin{aligned}
\mathbb{L}_F(s) &= \mathbb{E}[exp(-sF)] && (2.5)\\
&= \mathbb{E}\left[exp(-\sum_{x_i \in \phi} sg(x_i))\right] && (2.6)\\
&= \mathbb{E}\left[\prod_{x_i \in \phi} exp(-sg(x_i))\right] && (2.7)\\
&= \mathcal{P}_\phi(exp(-sg(x))) && (2.8)
\end{aligned}$$

Campbell's Theorem

Theorem 1 *Let Φ be a PP defined over $\mathbb{R}^d$ and $f : \mathbb{R}^d \to \mathbb{R}$, then:*

$$\mathbb{E}\left(\sum_{x_i \in \phi} f(x_i)\right) = \int_{\mathbb{R}^d} f(x)\Lambda(dx) \tag{2.9}$$

2.1.2 Types of Point Process

Poisson Point Process

Poisson Point Process (PPP) is a PP where $\Psi(A)$ is Poisson distributed with rate $\Lambda(A)$ and where for any disjoint sets $A_1, ..., A_k \in \mathbb{R}^d$, $\Psi(A_1), ..., \Psi(A_k)$ are independent Poisson random variables, i.e. for $n_1, ..., n_k \in \mathbb{N}$:

$$\mathbb{P}(\Psi(A_1) = n_1, ..., \Psi(A_k) = n_k) = \prod_{i=1}^{k} e^{-\Lambda(A_i)} \frac{\Lambda(B_i)^{n_i}}{n_!} \tag{2.10}$$

An homogeneous Poisson Point Process (HPPP) is a PPP whose intensity is uniform, its density can then be expressed as:

$$\Lambda(A) = \lambda|A| \tag{2.11}$$

Each point x_i of an HPPP is uniformly distributed inside A.
The PGFL of a Poisson Point Process is expressed as:

$$\mathcal{P}_\phi(f) = exp\left(-\int_{\mathbb{R}^d}(1-f(x))\Lambda(dx)\right) \tag{2.12}$$

The Poisson Point Process can be considered as the most popular PP for wireless networks modelling due to a simple PGFL expression and to the different existing theorems.

Binomial Point Process

Binomial Point Process (BPP) is a set of n i.i.d. points $x_i \in B \subset \mathbb{R}^d$. The BPP is the subset of points $x_i \in A \subset B$. The number of points in the BPP follows then a binomial distribution:

$$\mathbb{P}(\Psi(A)=k) = \binom{n}{k}\left(\frac{|A|}{|B|}\right)^k\left(1-\frac{|A|}{|B|}\right)^{n-k} \tag{2.13}$$

2.1.3 Properties of the Poisson Point Process

Thinning

The thinning ϕ^p of a PPP ϕ with a retention function $p(x)$ is a selection process such that each point $x_i \in \phi$ is selected with a probability $p(x_i)$. ϕ^p yields a PPP of density measure $p(x)\lambda(x)$.

Void probability

The void probability has been defined previously, for a PPP, the void probability is equal to:

$$v_\phi(A) = exp(-\Lambda(A)) \tag{2.14}$$
$$= exp(-\lambda|A|) \text{ for an homogeneous PPP} \tag{2.15}$$

The contact distribution defined the probability that for a PPP ϕ, $\psi \neq 0$ for a given subset A. It is closely related to the void probability by:

$$C_\phi(A) = 1 - v_\phi(A) \tag{2.16}$$

Distance to the nth neighbour

For a PPP defined on the 2-dimensional Euclidean space $\mathbb{R}^2$, the probability distribution function of the distance r to n^{th} closest point $x_i \in \phi$ from the center is given by:

$$f_R(r,n) = \frac{2(\pi\lambda)^n}{(n-1)!}r^{2n-1}exp(-\lambda\pi r^2) \tag{2.17}$$

Probability Generating Function of a Poisson Point Process

The PGFL for any real positive function f over $\mathbb{R}^d$ and for a PPP ϕ of intensity Λ is:

$$\mathcal{P}_\phi(f) = exp\left(-\int_{\mathbb{R}^d}(1-f(x))\Lambda(\mathrm{d}x)\right) \tag{2.18}$$

For an homogeneous PPP, $\Lambda(\mathrm{d}x) = \lambda dx$, the PGFL is:

$$\mathcal{P}_\phi(f) = exp\left(-\lambda\int_{\mathbb{R}^d}(1-f(x))\mathrm{d}x\right) \tag{2.19}$$

Similarly, for a random variable $F = \sum_{x_i\in\phi} g(x_i)$ with ϕ being a PPP, the Laplace transform is:

$$\mathbb{L}_F(s) = exp\left(-\int_{\mathbb{R}^d}(1-sg(s))\Lambda(dx)\right) \tag{2.20}$$

Finally, let us compute the Laplace transform for a case that will be used in the following parts: a HPPP over $\mathbb{R}^2$ for which the intensity in polar coordinates is $\Lambda(r\mathrm{d}r\mathrm{d}\theta) = \lambda r\mathrm{d}r\mathrm{d}\theta$.

$$\mathbb{L}_F(s) = exp\left(-2\pi\lambda\int_r(1-sg(s))r\mathrm{d}r\right) \tag{2.21}$$

2.2 Probability fundamentals

In the following, probability notions that will be widely used in the work are stated.

2.2.1 The central limit theorem

[25] Let $X_1, X_2, ..., X_n$ be independent and identically distributed random variables where $\mathbb{E}[Y_i] = \mu$ and $Var(Y_i) = \sigma^2$. Define:

$$U_n = \frac{\sum_{i=1}^n Y_i - n\mu}{\sigma\sqrt{n}} \tag{2.22}$$

Then the distribution function of U_n converge to the standard normal distribution as $n \to \infty$. That is:

$$\lim_{n\to\infty}\mathbb{P}(U_n \le u) = \int_{-\infty}^{u}\frac{1}{\sqrt{2\pi}}exp\left(-t^2/2\right)\mathrm{d}t \tag{2.23}$$

2.2.2 The moment generating function and the characteristic function

Let X a random variable. The moment generating function of X is defined by:

$$m_X(t) = \mathbb{E}[exp(tX)] \tag{2.24}$$

The following relation between the moment generating function of X and the Laplace transform of $f_X(x)$ (the pdf of X) hold :

$$m_X(t) = \mathcal{L}_{f_X}(-t) \tag{2.25}$$

The characteristic function of X is defined by:

$$\phi_X(t) = \mathbb{E}[exp(jtX)] \tag{2.26}$$

The following relation between the characteristic function and the moment-generating function holds:

$$m_X(t) = \phi_X(-jt) \tag{2.27}$$

2.3 Reconfigurable Impedance Surfaces: Fundamentals

The Reconfigurable Impedance Surfaces (RIS) is one of the device used in the reflective radio technology which aims at enabling more paths than only the Line-of-Sight (LoS) path. Reflective devices (here RIS's) will be placed in the environment of communication such that they allow an incident wave from the transmitter to be reflected towards the receiver, as in the figure 2.3, to create a Non Line-of-Sight path (NLoS) .
This may come useful in situations where the LoS path is blocked or is much more attenuated than the NLoS path. But also, if there is a large number of RIS's that can be tuned to be received coherently with the signal from the LOS path, this can lead to an increase of the received power and therefore to the channel capacity which would allow to have a system with a higher data rate.

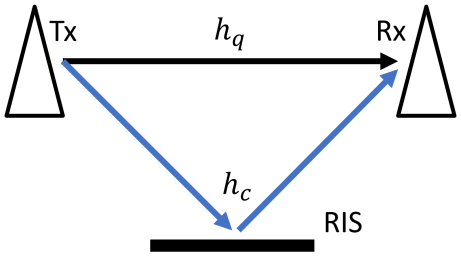

Figure 2.1: Reflective Radio Technology concept

2.3.1 Motivations

In order to cope with the increasing demand of data transmission, the fifth generation of wireless communications and the previous generation were mainly focused on optimizing the communication only at the end points (the transmitter and the receiver) while considering that the wireless environment between the end points can't be controlled in any way.
Nevertheless, for the 6th generation (6G) of wireless communications, because of the new applications and scenarios for wireless communications, such as the Internet of Things, but also the need of improving the coverage to avoid any dead-zone, massive MIMO transceivers may not be an efficient solution in every situation because of their cost, their energy consumption and their size.
The Reconfigurable Impedance Surfaces (RIS) can be a solution to partly replace the use of massive MIMO transceivers as they are small-sized for high frequency communications (above 1 GHz), they can be nearly passive and they are predicted to reduce the cost of the system compared to one that uses more classical MIMO elements.

2.3.2 Hardware architecture

The two main categories of RIS are the active and the passive RIS:

- The term "active RIS" is used to classify an RIS which uses heavy signal processing units or high power RF circuits that are parts of the RIS. The main type of active RIS are the metasurface antennas which act as a relay and can also be used as transceiver at an UE or a BS. They consist in an array of sub-wavelength metasurface radiators connected by a waveguide.

  However because of its design which does not only aim to be used as reflective design, an active RIS generally has a poor energy efficiency when used as such. This is the reason why they will not be used in this work.

- The term "passive RIS" is used to classify an RIS which does not use any RF amplifier circuit and use only light signal processing unit which is why some authors also use the term "nearly-passive RIS" [22]. The possibility of using energy-harvesting module to supply signal processing unit has also been studied which would enable the RIS to increase the coverage without any increase of energy consumption.

  The passive RIS is a two-dimensional structure whose size is much larger than the wavelength. It thickness should be much thinner than the wavelength. Each element of this RIS is composed

of metallic or dielectric patches (also called "metasurfaces") printed on substrate which offers a passive scattering. Those metasurfaces allow the polarization and the angle of the reflection to be controlled through a micro-controller.

An example of fabricated RIS is available on figure 2.3.2 with the resonators on each element, the phase shifters and the FPGA controller.
Patch antennas using metasurfaces were already studied and tested in the early 2010's [28] [4], but those antennas were mainly designed as transceiver elements. The idea of using metasurfaces to build reflective element came with the emerging concept of "smart-radio-environment" (ie: controlling the environment of the transmission).
A main work where a metasurface-based RIS has been designed, build and measured is [3]. Their results the directivity of an RIS and how accurate the tuning of the radiation pattern can be. However, this RIS uses 2-bit phase shifting elements, thus the phase shift of each element has only $90\,\mathrm{deg}$ resolution. Also this RIS only has a $\pm 60\,\mathrm{deg}$ angular range which limits the cases where it can be used depending on its location, and the locations of the UE and the BS.

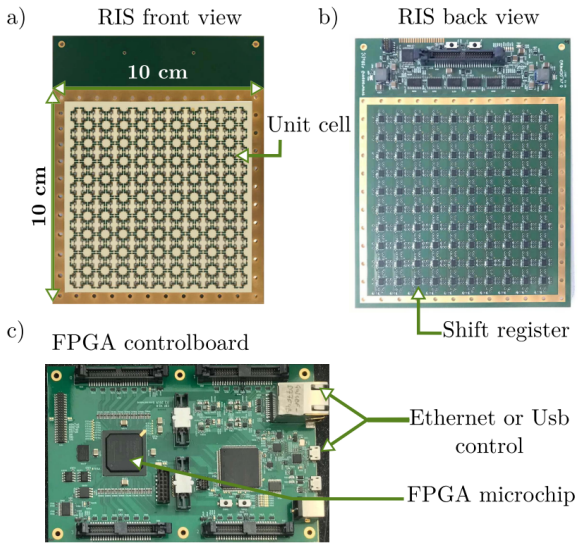

Figure 2.2: RIS fabricated in [7]

2.3.3 RIS-aided wireless networks

The first influential paper presenting the idea of using passive RIS in wireless network is [10] where the goal was to investigate an energy-efficient solution to provide a link between a UE and a BS when the LoS link is blocked by an obstacle. This work can be seen as refinement of the idea of using large intelligent surfaces [8] or passive intelligent mirrors [11] in a wireless networks to overcome blockages. However in [10], the idea of having reconfigurable surfaces depending on the location of the UE and the BS is tackled. Both papers [8] and [11] present the concept of using controlled reflection in a MIMO framework which aims at massively increasing the spatial diversity by increasing the number of transceivers.
[17] and [9] are other early papers which investigate the use of RIS in wireless communications. Their contributions are both on beamforming algorithms for the RIS to optimize the transmissions. It is to be noted that [17] couples the RIS with UAVs (unmanned aerial vehicles) transceivers, the beamforming algorithm then takes into account a moving transceiver, which challenges the configuration of the RIS.

2.3.4 Propagation model

Ideally, one should model the scattering on each element independently to obtain an accurate model of the reflection of a wave through the RIS. However, depending on the context, this approach can be too complex for a large number of element and irrelevant as some only needs simpler approximation models. In the following, a few different propagation models will be listed:
In [23], different models of path loss of wave scattered by an RIS are developed for different cases by taking into account the radiation pattern of each element of the RIS. Measurement are made to validate the models in different conditions. These models all take into account that the phase shift of each element is optimized:

- If the transmitter and the receiver are both in the far-field of the RIS:

$$PL = \frac{64\pi^3(rd)^2}{G_t G_r G M^2 N^2 d_x d_y \lambda^2 F(\theta_t, \phi_t) F(\theta_r, \phi_r) A^2} \tag{2.28}$$

Where r is the distance transmitter-RIS, d is the distance RIS-receiver. G_t G_r and G are the antenna gain from the transmitter, the receiver and the gain of an element. M and N are the number of elements in each row and each column in the array. d_x, d_y are the horizontal and the vertical length of an element. λ is the wavelength. F is the radiation pattern of an element which can have different expressions depending on the configuration of the RIS. θ_t and θ_r are the elevation angle of the incident wave and the reflected wave. ϕ_t and ϕ_r are the azimuth angle of the incident and the reflected wave. A represents the coefficient of reflection of an element.

- If either the transmitter and the receiver are both in the far-field of the RIS or only one of them:

$$PL = \frac{64\pi^3}{G_t G_r G d_x d_y \lambda^2 A^2 |\sum_{m=1-\frac{M}{2}}^{\frac{M}{2}} \sum_{n=1-\frac{N}{2}}^{\frac{N}{2}} \frac{\sqrt{F_{n,m}^{combine}}}{r_{n,m}^t r_{n,m}^r}|^2} \tag{2.29}$$

Where $F_{n,m}^{combine}$ models the radiation pattern of the transmitter antenna, the receiver antenna an the element (n, m) of the RIS. $r_{n,m}^t$ and $r_{n,m}^r$ denotes the distance between the element (n, m) and respectively the transmitter and the receiver antenna.

- If either the transmitter and the receiver are both in the far-field of the RIS or only one of them and the RIS has a much larger width and height than the wavelength:

$$PL = \frac{16\pi^2(r+d)^2}{G_r G_t \lambda^2 A^2} \tag{2.30}$$

In [26], the authors used a similar development than the one leading to the equation 2.29 but the concept of radar-cross section (RCS) has also been used, leading to the expression of the received power:

$$PL = \frac{P_t}{16\pi^2 \eta_r} |\sum_{m=1}^{M} \sum_{n=1}^{N} \frac{\sqrt{G_t G_r} \sigma_{m,n} exp(j(\phi_{m,n} + \Phi_{m,n})^2}{r_{m,n}^t r^r m, n}| \tag{2.31}$$

Where η_r is the efficiency of the receiving antenna, $\sigma_{m,n}$ is the radar cross section of the element (m, n). $\phi_{m,n}$ is the phase shift of the element (m, n). $\Phi_{m,n}$ is the phase shift of the element (m, n) caused by the propagation delay.
In [31] the authors have derived a path loss model using physical optics techniques and have also introduced a way to use this model in communications oriented analysis. This model is :

$$P_r = \frac{1}{2\eta}(\frac{ab}{\lambda})^2 (\frac{P_t G_t \eta}{2\pi r_i^2})^2 (\frac{cos(\theta_t)}{d^2} (sinc(\frac{\pi b}{\lambda}(sin(\theta_r) - sin(\theta_s))))^2 \frac{\lambda^2 G_r}{4\pi} \tag{2.32}$$

a and b being the height and the length of the RIS, η the medium impedance and θ_s the aimed reflection angle.

2.3.5 Further possible advancement

When investigating the literature, the fabrication of the RIS's seems to be a challenge that is about to be solved as successful prototypes are already tested. However, standardization is still to be done. In 2022, regional standard developing organisations are already studying the integration of RIS's in wireless communication networks [13]. It is also predicted that 3GPP would start the standardization of RIS's by 2023, if they are planned to be deploy in the second stage of 5G. However, as they are still modelling challenges (presented below), it could be likely that the RIS's will only be standard for 6G, around the 2030s.
The major challenges to overcome lie in the "system analysis" field, some example are:

- Even if some path loss models have been presented in the section above. They are either too complex or inaccurate in some aspects to be used in a budget link analysis. For instance equation 2.30, does not take into account the angle of reflection and incidence, but measures from [3], shows that an RIS has a given angular range.
- At the moment, not any limit of performance of an RIS-aided wireless network have been studied.
- The influence of the mobility of the UE should also be studied. As the RIS should be designed be very directive, a moving UE should force the RIS to continuously update its tuning.
- Analysis on large-scale RIS-aided wireless networks should also be done the match with real scenarios and investigating the impact of the RIS in a realistic system.

2.4 Stochastic Geometry and Reconfigurable Impedance Surfaces

This section will consist in a list of work describing a stochastic geometric analysis of an RIS-aided network and a brief description of their contributions.

2.4.1 Spatial diversity

In the following papers, the advantages of using RIS's in a wireless network to increase the spatial diversity is studied, bye adding a second non line-of sight link to the already present LoS link.
In [12], the authors analyse the coverage and the channel hardening of a wireless network with an RIS and where the channel fading gain is modelled as being Nakagami-m distributed. The major contribution is the use of the Gil-Peleaz inversion to combine the Line-of-Sight (LoS) link and the non Line-of-Sight (NLoS) link going through the RIS by computing the characteristic function of their channel.
In [20], the effectiveness of the RIS's to counteract the increased path loss from which suffers the mm-Wave communication is studied both analytically and by simulation. As the wireless network is modelled as being blockage-free, the possibility of adding the LoS link and one NLoS passing by an RIS is developed to enhance the coverage. Both the RIS's and the base stations (BS's) have been modelled as point processes and it has been shown that the SIR coverage depends on the density of BS's, the density of RIS's, the number of elements on an RIS and the number of isotropic elements. Thus, deploying RIS's should be as effective than deploying more active antenna on each BS. Finally, their results show that a certain ratio of RIS's to BS's should be exceeded in order to get a NLoS link that offers a better coverage than the LoS link.

2.4.2 Impact of the RIS on interferences

The use of RIS's in a wireless network could bring the issue that the interferences are also reflected and enhanced by the RIS's. However, the general conclusion of the following studies are that the interference amplification is less strong than the signal enhancement.

In [32], the authors investigate an RIS-aided non-orthogonal multiple access (NOMA) system. They provide closed-form expressions of the coverage probability and the ergodic rate of an RIS-aided NOMA system and show the improvement brought by the RIS's as well analytically than with simulations. The system model used there also contains blockages and interference from other base stations. They consider channels impacted by Nakagami-m distributed channel fading gain but the possibility of using the LoS link with the NLoS link is not investigated.
The two main differences between this work and the paper [32] which also models a wireless network with RIS's, interferences and blockages are that here the possibility of using multiple uniformly-distributed RIS's at the same time will be investigated and multiple association rules involving a network with multiple BS will be compared in a case where blockages are present in the network.
In [16], the propagation of the interference by the RIS is investigated in the millimeter wave range. It is shown that this type of interference stays inferior to the LOS interference and does not overshadow the RIS-aided signal link. Besides, it is also shown that the far-field waves equation stays relevant a non-negligible part of the near-field. No specific channel small-scale fading gain is used but instead, an absorption coefficient $exp(-\kappa(f)r)$, as at THz frequency this coefficient is not negligible and should therefore be taken into account.
In [14], a system where both the RIS's and the BS's are modelled as PPPs. A transmission uses all the RIS's located in a given sector (called "capture area") around the used BS. The metric of performance used there is the average SINR and not the coverage as other papers. The impact of the RIS's on the interfering signal is also studied and a lower bound of the interference power is derived by averaging the interference power and neglecting any correlations between the different terms of interference. They also introduce the notions of knee point of a capture area. This knee point describes the size of the capture area at which the SNR enhancement from the RIS's starts to increase drastically.
The authors of [29] have modelled a wireless network where both the BS's and the RIS's are represented by PPPs. This system also contains blockages which are taken into account by removing or not a link between two points with a certain probability. When an RIS is used to transmit a signal, only one RIS can be used and no small-scale fading are present in the model. This work is axed on the impact on the SINR of the reflection of the interference by the RIS's. When considering those interference reflected by RIS's, the SINR enhancement brought by the RIS's does not always increase when the density of RIS's increases and the need of optimizing the placement of the RIS's depending on the density of blockage, of BS's or the directivity of the RIS's is highlighted.
In [18] a network where only one RIS is used to transmit the signal is modelled. This network is impacted by interference which can also be reflected by an RIS. The outage probability is investigated but their main contribution is analysing the spatial throughput ($bits/Hz/km^2$) compared to the total cost of the network for different ratio of RIS's over BS's. It is shown that the addition of RIS's allows to increase the power of signal while only marginally increasing the power of interference. Their results also show that a linear growth of the spatial throughput compared to the cost of the network can be expected thanks to the use of RIS's.

2.4.3 RIS to handle blockages

The use of RIS's in a network to handle blockages has been studied in some papers [32], [29] or [33] as they are an intuitive use of the RIS's but the blockages were not the main focuses.
In [15], the main focus is to study the use of RIS's to avoid any blind spots (non-covered locations) in wireless network including obstacles. The BS's, the UEs and the obstacles are all modelled by PPP and a given fraction of obstacles are equipped with RIS's on their surfaces. The main contributions are the computation of a visibility probability when no small-scale fading gain are present and a complete framework to model a network with RIS's and obstacles, framework which will be used in the last part of this work.

2.4.4 Physical security layer

The following work analyses another way to use the RIS's by not wanting to control the environment to enhance the communication but by using the RIS's to aim the waves at the designated user.
The authors of [33] evaluate an RIS-aided wireless network aimed to improve the security of the transmission in a MIMO communication system. The "Physical Layer Security" regroups different technique designed to reduce the signal leakage to eavesdroppers. The use of RIS's allows a steering of the beam towards the user with a certain accuracy. The outage probability is also investigated to study the consequence of using RIS's to overcome blockages. The analyse is mode only considering the use of either the LoS or the NLoS path. The results show that the outage probability decrease when the transmit power or the number of elements on an RIS increases, they show that the lower the LoS path-loss exponent is, the greater the number of element on an RIS should be in order to have a better outage probability on the NLoS link than on the LoS link. Finally, it has been shown that the secret outage probability decreases when the number of element of an RIS increases or when the antenna of the BS has a radiation pattern with a narrower radiation pattern.

2.4.5 Optimization of an RIS-aided network

This problem of placement of the RIS's is tackled in [6] while not considering the interferences but only the blockages. It has been shown that for sparse blockage, a distance between the RIS's and the BS's similar to the radius of the cell is optimal, while for dense blockages it is more optimal to have a distance of a half of the radius of the cell. The importance of mounting RIS's at intersections of road in an urban environment has also been shown.

2.4.6 Advantages compared to other techniques

In [30] a comparison is made between the use of an RIS or decode-and-forward relay in order to forward the signal from the transmitter to the receiver. The two main performance of metrics used are the outage probability and the energy efficiency. It is shown that the use of RIS's generally outperforms the use of relay in terms of energy efficiency as the RIS is only composed of passive elements. It is also shown that with a number of elements high enough, the RIS also outperforms the decode-and-forward relay on the outage probability.

Chapter 3

On the joint use of multiple RIS in wireless networks

3.1 Introduction

This chapter aims at investigating the performance, mainly the coverage, of a wireless system in which the transmitter can use multiple RIS's along with the LoS link to increase the received SINR under Nakagami-m distributed small-scale fading.

3.2 System Model

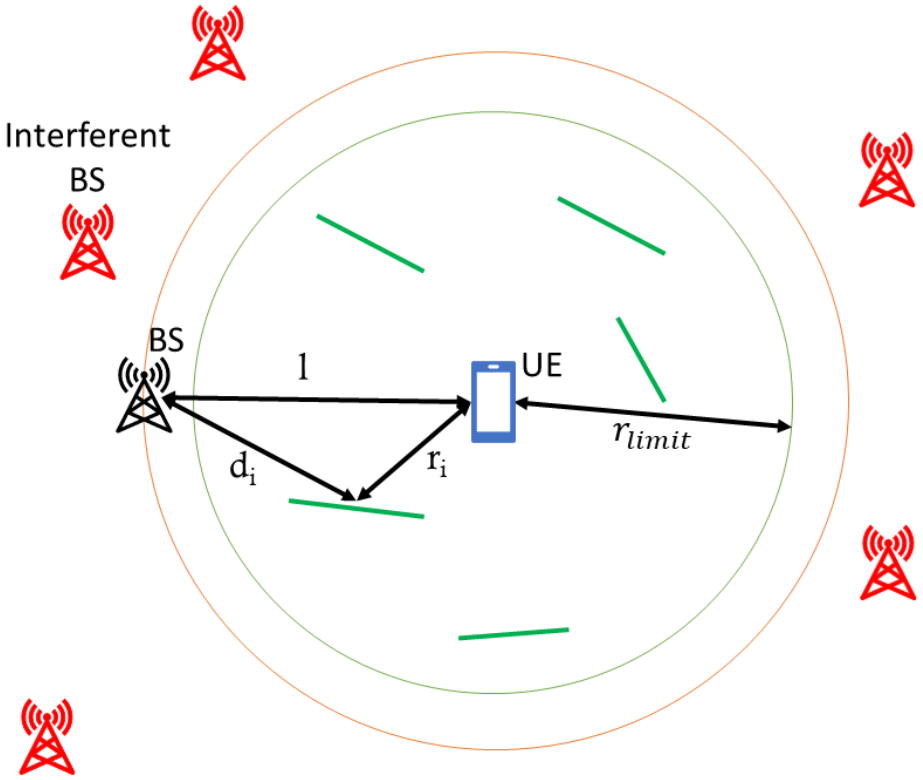

Figure 3.1: System Model Scheme

In this model, a UE will transmit data to the closest BS, located at a known distance l as represented

on figure 3.1. To enhance the performance, multiple RIS's are available. These are modelled by a PPP with a density λ_{RIS} and are located inside a disk of radius r_{limit}. Each RIS will have N elements, the distance between the UE and the ith RIS will be r_i and the distance between the ith RIS and the BS will d_i. The last elements of this model are interferent BS's located outside the disk of radius l and centered around the UE. These BS's will be modelled as PPP of density $\lambda_i(x) = 0$ if $x < l$ and $\lambda_i(x) = \lambda_{BS}$ if $x > l$.
Three types of link will be denoted :

1. The LoS link UE-BS
2. The NLoS link UE-RIS
3. The NLoS link RIS-BS

All the links will be impaired by a small-scale fading gain following the same Nakagami-m distribution of parameter m and of mean fading power Ω. It is worth noting that in this works $\Omega = 1$ as none of the element between the UE and the BS should amplify the waves.
From [12], two channel gains will be used to compute the received:

- The channel gain $|h_q|$ representing the LoS link which is expressed:

$$|h_q| = \left(\frac{\lambda}{4\pi}\right) \varepsilon_q l^{-\alpha/2} \tag{3.1}$$

  where λ is the carrier wavelength, ε_q represents the channel fading gain on the LoS link and α is the path loss exponent.

- The channel gain $|h_c|$ represents the NLoS link going through the RIS. Here an important assumption is made that the phase shift of each element are set such as the received signals that have been reflected by each of the N elements are coherent and therefore their signal power can be added without considering the position of each of the element on the RIS. The channel gain $|h_c|$ is expressed:

$$|h_c| = \left(\frac{\lambda}{4\pi}\right) (r+d)^{-a/2} \sum_{k=1}^{N} \varepsilon_{g,k}\varepsilon_{h,k} \tag{3.2}$$

  This propagation model comes partly from [23] but also takes into account the channel fading gains. r and d represents the distance from the UE to the RIS and from the RIS to the BS. $\varepsilon_{g,k}$ is the channel fading gain of the link from the UE to the kth element of the RIS and $\varepsilon_{h,k}$ is the channel fading gain from the kth element of the RIS to the BS.

The assumption is here made that the signal from the LoS and the NLoS link are coherent, then the signal power S is written:

$$S = P(|h_q| + |h_c|)^2 \tag{3.3}$$

Only the LoS interferences are here considered and the channel gain of the interference will have the expression 3.1.
Finally, additive white gaussian noise will be added, whose variance [12] is given by:

$$\sigma^2_{N_0} = -174dBm/Hz + 10log_{10}(BW) + 10dB \tag{3.4}$$

where BW represents the used bandwidth.

3.3 Coverage probability without interference

This section will contain the development and the validation of results for the expression of the coverage probability without considering yet the interference. This will be made progressively by adding the different features of the system:

1. Considering that only one RIS is used and that its location is known.
2. Considering that one RIS is used but its location is not known.
3. Considering that a known number number of RIS's are used and are randomly placed.
4. Modelling the RIS's by a PPP and have a random number of used RIS's.

3.3.1 One RIS with known location

The coverage is given by the probability that the received SNR is higher than a given threshold θ, knowing the signal power S from the equation 3.3. As $|h_c|$ and $|h_q|$ are the only random factors as they contain the small-scale fading gains, the coverage probability is given by:

$$\mathbb{P}\left(\frac{S}{\sigma^2_{N_0}} > \theta\right) = \mathbb{P}\left(\frac{P(|h_q| + |h_c|)^2}{\sigma^2_{N_0}} > \theta\right) \tag{3.5}$$

$$= \mathbb{P}\left(|h_q| + |h_c| > \sqrt{\frac{\theta\sigma^2_{N_0}}{P}}\right) \tag{3.6}$$

$$= 1 - F_T\left(\sqrt{\frac{\theta\sigma^2_{N_0}}{P}}\right) \tag{3.7}$$

where $T = |h_c| + |h_q|$, F_T represents the cdf of T.
To characterize the distribution of the random variable T, the following property will be used: if X and Y are independent RVs, the characteristic function of $X + Y$ is given by the product of the CF of X and the CF of Y. This property will be used here to compute T, because the channel of the LoS link $|h_c|$ and the NLoS link $|h_q|$ are independent as their small scale fading gain are independent. In the following, the CF of $|h_q|$ and $|h_c|$ are developed.
As shown at the expression 3.1, $|h_q|$ is a Nakagami-m distributed RV multiplied by a known factor, then the CF $\phi_{|h_q|}(\omega)$ is written using the definition of the CF:

$$\phi_{|h_q|}(\omega) = \mathbb{E}\left[exp(j\omega|h_q|)\right] \tag{3.8}$$

$$= \mathbb{E}\left[exp(j\omega\left(\frac{\lambda}{4\pi}\right)\varepsilon_q l^{-\alpha/2})\right] \tag{3.9}$$

$$= \phi_{\varepsilon_q}\left(\omega\left(\frac{\lambda}{4\pi}l^{-\alpha/2}\right)\right) \tag{3.10}$$

As ε_q is a Nakagami-m distributed RV of parameter m and of mean fading power Ω, its CF can be found in [12]:

$$\phi_{|h_q|}(\omega) = \phi_{\varepsilon_q}\left(\omega\left(\frac{\lambda}{4\pi}l^{-\alpha/2}\right)\right) \tag{3.11}$$

$$= \frac{1}{\sqrt{\pi}}\Gamma(m+0.5)\left(U\left(m, 0.5, \frac{-\left(\omega\frac{\lambda}{4\pi}l^{-\alpha/2}\right)^2\Omega}{4m}\right)\right)^* \tag{3.12}$$

where $\Gamma(x)$ is the gamma function and $U(a, b, z)$ is the confluent hypergeometric function.

Following the same argument than the one used the compute the expression 3.10 and while also making the assumption that the small-scale fading gains related to each element of the RIS $\varepsilon_{g,k}$ and $\varepsilon_{h,k}$ are independent and identically distributed for $k = 1, ..., N$, the CF of $|h_c|$ is:

$$\begin{aligned}
\phi_{|h_c|}(\omega) &= \mathbb{E}\left[exp\left(j\omega\frac{\lambda}{4\pi}(r+d)^{-a/2}\sum_{k=1}^{N}\varepsilon_{g,k}\varepsilon_{h,k}\right)\right] && (3.13)\\
&= \prod_{k=1}^{N}\mathbb{E}\left[exp\left(j\omega\frac{\lambda}{4\pi}(r+d)^{-a/2}\varepsilon_{g,k}\varepsilon_{h,k}\right)\right] && (3.14)\\
&= \left(\phi_{\varepsilon_g\varepsilon_h}(j\omega\frac{\lambda}{4\pi}(r+d)^{-a/2})\right)^N && (3.15)
\end{aligned}$$

The RV $\varepsilon_g\varepsilon_h$ is a product of two identically distributed Nakagami-m RVs with parameter m and mean fading power Ω, its CF can also be found in [12]:

$$\begin{aligned}
\phi_{|h_c|}(\omega) &= \left(\phi_{\varepsilon_g\varepsilon_h}(j\omega\frac{\lambda}{4\pi}(r+d)^{-a/2})\right)^N && (3.16)\\
&= \left(\frac{1}{\sqrt{\pi}\left(\Gamma(m)\right)^2}G_{2,2}^{2,2}\left[\frac{4}{s^2}\left(\frac{m}{\Omega}\right)^2\middle|\begin{matrix}1/2 & 1\\ m & m\end{matrix}\right]\right)^N && (3.17)
\end{aligned}$$

where $s = j\omega\frac{\lambda}{4\pi}(r+d)^{-a/2}$ and $G_{2,2}^{2,2}$ is the Meijer-G function.
By having the CF of $|h_q|$ and $|h_c|$, it is possible to compute the CF of T with the following identity:

$$\phi_T(\omega) = \phi_{|h_q|}(\omega)\phi_{|h_c|}(\omega) \quad (3.18)$$

The equation of the outage probability 3.7 depends on the cdf of T. The cdf of T can be computed from the CF by using the Gil-Pelaez inversion law:

$$F_T(t) = \frac{1}{2} - \frac{1}{\pi}\int_0^\infty Im\left[exp(-j\omega t)\phi_T(\omega)\right]\omega^{-1}\mathrm{d}\omega \quad (3.19)$$

Validation of the outage probability

This derivation of the coverage probability can be validated by comparing it with Monte-Carlo simulations of the same scenario where the only RV sampled are the channel fading gains.
Two sets of parameters have been used, one which makes the received power from the LoS link higher than from the NLoS link and one which makes the received power from the NLoS link higher than from the LoS link. Both of those sets of parameters have been tested for different values of the parameter m of the Nakagami-m distributions.
For the first set of parameters which makes the LoS link stronger, $P = 2W$, $l = 100m$, $r = 200m$, $d = 293m$, $\alpha = 4$, $BW = 10MHz$, $\lambda = 16.67cm$ and $N = 10$. Parameters m of 0.5, 1 and 2 are tested and the outage probability is compared with the Monte Carlo simulations.
For the second set of parameters which makes the LoS link more important, $P = 2W$, $l = 550m$,$r = 55m$, $d = 550m$, $\alpha = 4$, $BW = 10MHz$, $\lambda = 16.67cm$ and $N = 100$. Parameters m of 0.5, 1 and 2 are tested and the outage probability is compared with the Monte Carlo simulations.
When comparing the theoretical values and the values from the simulations on figure 3.2 and 3.3, no important differences can be seen. It is also worth noting that the shape of the curves on figure 3.2 and 3.3 are different, which highlights the fact that the LoS and NLoS channel gains follow different distributions. The use of the RIS results in a sharper coverage probability, which means that the channel gain are less spread, "the environment is more controlled" which can be related to the concept of smart radio environment presented before. This phenomenon is called "channel hardening" in [12].

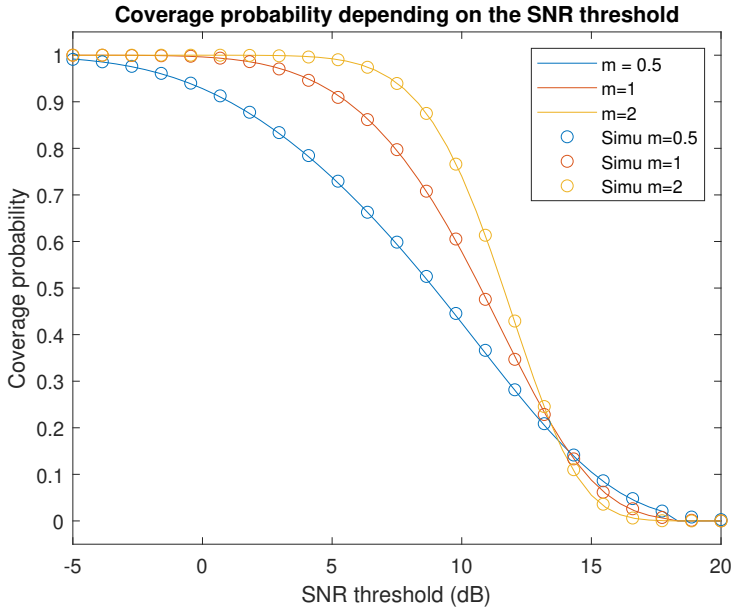

Figure 3.2: Validation of the coverage probability for an important LoS link

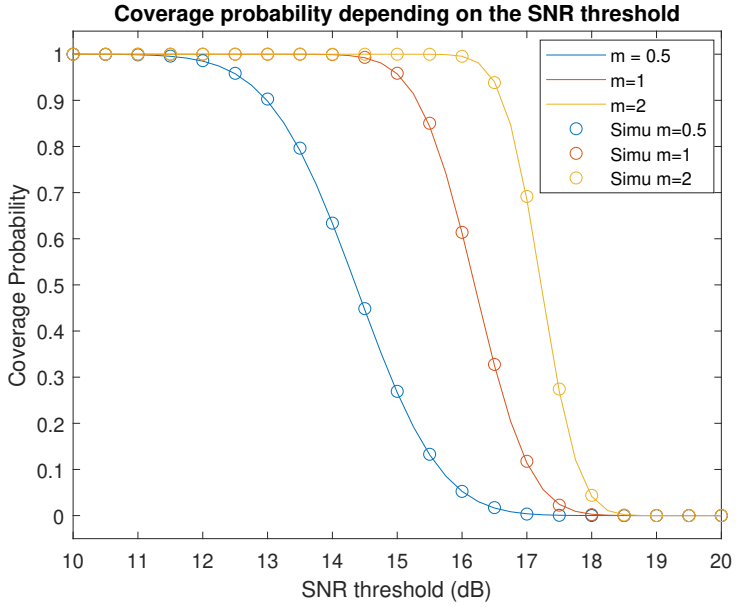

Figure 3.3: Validation of the coverage probability for an important NLoS link

3.3.2 One RIS with random location

When the used RIS has a random location inside a disk of radius r_{limit}, the only difference from the previous computation is that d and r become random. Two RVs will then be introduced: r, the distance UE-RIS and β the angle BS-UE-RIS. Those RVs are enough to express d the distance UE-RIS-BS:

$$d(r,\beta) \quad = \quad \sqrt{r^2 + l^2 - 2rl\cos(\beta)} \tag{3.20}$$

In $\phi_T(\omega)$, only the term $\phi_{|h_c|}(\omega)$ depends on r and $d(r,\beta)$. In order to compute the average coverage

probability, one should take the expected value of $\phi_{|h_c|}(\omega)$ over the two RVs r and ϕ. To do so, the probability density function of the RVs is needed.
As the RIS is uniformly distributed inside a disk of radius r_{limit}, the angle β will be uniformly distributed over 2π and its pdf is $f_\beta = \frac{1}{2\pi}$. The cdf of r can be easily computed, the probability that the RIS lies inside a disk of radius r is $\frac{r^2}{(r_{limit})^2}$. However, the model of path loss used $(r+l)^{-\alpha/2}$ can lead to an infinite gain if r (and d) are close to zero. Thus, the zone where the RIS can be located will be represented as a ring of in radius of $1m$ and of outer radius of r_{limit}, which transforms the cdf of r into $\frac{r^2}{(r_{limit})^2} - 1$. Then the pdf is derived by taking the derivative on r:

$$\begin{aligned} f_R(r) &= \frac{d}{dr}\left(\frac{r^2}{(r_{limit})^2 - 1}\right) && (3.21)\\ &= \frac{2r}{(r_{limit})^2 - 1} && (3.22)\end{aligned}$$

The expression 3.17 becomes when taking the expected value on r and β:

$$\begin{aligned} \phi_{|h_c|}(\omega) &= \mathbb{E}\left[\left(\frac{1}{\sqrt{\pi}\left(\Gamma(m)\right)^2} G_{2,2}^{2,2}\left[\frac{4}{s^2}\left(\frac{m}{\Omega}\right)^2 \middle| \begin{matrix} 1/2 & 1 \\ m & m \end{matrix}\right]\right)^N\right] && (3.23)\\ &= \int_1^{r_limit} \int_{-\pi}^{\pi} \left(\frac{1}{\sqrt{\pi}\left(\Gamma(m)\right)^2} G_{2,2}^{2,2}\left[\frac{4}{s^2}\left(\frac{m}{\Omega}\right)^2 \middle| \begin{matrix} 1/2 & 1 \\ m & m \end{matrix}\right]\right)^N f_\beta(\beta) f_R(r) \mathrm{d}\beta \mathrm{d}r && (3.24)\\ &= \int_1^{r_limit} \int_{-\pi}^{\pi} \left(\frac{1}{\sqrt{\pi}\left(\Gamma(m)\right)^2} G_{2,2}^{2,2}\left[\frac{4}{s^2}\left(\frac{m}{\Omega}\right)^2 \middle| \begin{matrix} 1/2 & 1 \\ m & m \end{matrix}\right]\right)^N \frac{1}{2\pi} \frac{2r}{(r_{limit})^2 - 1} \mathrm{d}\beta \mathrm{d}r && (3.25)\end{aligned}$$

where $s = j\omega\frac{\lambda}{4\pi}(r + d(r,\beta))^{-a/2}$

Far-Field approximation

If $r_{limit} << l$, the expression 3.20 could be approximated by:

$$d(r,\beta) \approx l \tag{3.26}$$

Which would make $d(r,\beta)$ independent of β and would allow to remove the integral on β in the expression of $\phi_{|h_c|}(\omega)$:

$$\phi_{|h_c|}(\omega) = \int_1^{r_limit} \left(\frac{1}{\sqrt{\pi}\left(\Gamma(m)\right)^2} G_{2,2}^{2,2}\left[\frac{4}{s^2}\left(\frac{m}{\Omega}\right)^2 \middle| \begin{matrix} 1/2 & 1 \\ m & m \end{matrix}\right]\right)^N \frac{2r}{(r_{limit})^2 - 1} \mathrm{d}r \tag{3.27}$$

However this approximation could lead to some non-negligible errors depending on the values used for r_{limit} and l, these errors will be studied during the validation of this subsection.

Validation

In order to validate the development concerning the position of the RIS becoming random, two situations will be analysed for the expression without far-field approximation. The difference between the scenario will be the radius of the zone of the RIS zone r_{limit}. Then, the validation of the far-field approximation will be made by comparing the analytical expression including the far-field approximation and Monte-Carlo simulations for multiple ratios r_{limit}/l to observe for which set of parameters this approximation can be considered as valid.

- For the first validation, the model without far-field approximation. The parameters for this simulation are $P = 2W$, $\alpha = 4$, $l = 550m$, $BW = 10MHz$, $\lambda = 16.67cm$, $N = 100$ and the m-parameter of the Nakagami distribution is $m = 0.5$. The limit of the RIS zone is either $20m$ or $100m$. As seen on figure 3.4, no noticeable difference can be seen between the evaluation of the analytic expression and the Monte-Carlo simulation results. That is the case for both the smaller and larger RIS zone. It is also interesting to see that the coverage probability becomes "sharper" for the smaller RIS zone, which, compared to what was observed in the previous subsection, means that the NLoS is more important than the LoS link. The opposite is also true when observing the coverage probability for $r_{limit} = 100m$ which makes the LoS link more important than the LoS link.

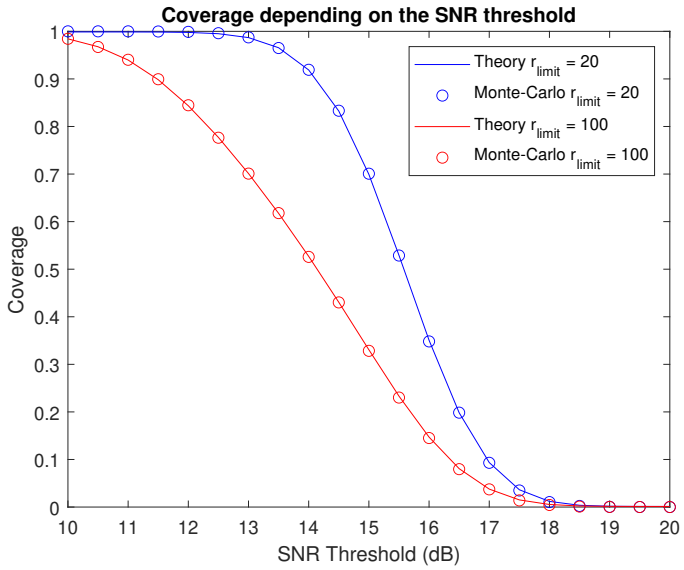

Figure 3.4: Coverage probability for a randomly located RIS, without far-field approximation

- For the second validation to observe the accuracy of the far-field approximation, the parameters for this simulation were: $P = 2W$, $\alpha = 4$, $l = 550m$, $BW = 10MHz$, $\lambda = 16.67cm$, $N = 100$ and the m-parameter of the Nakagami distribution is $m = 0.5$. r_{limit} takes different values depending on the ratio r_{limit}/l tested. Figure 3.5 represented the coverage probability for different SNR thresholds and different ratios r_{limit}/l. It can be seen that the analytic results (plain line) follow well the simulations (dashed line) up until $r_{limit}/l = 0.1$. For higher ratios, the far-field approximation overestimates the NLoS link as the curve is "sharper" than the curve from the simulations. This comes from the fact that the large r_{limit} compared to l, the expression 3.20 will often lead to a higher distance than l, and therefore the real NLoS link will be weaker. In conclusion, as the expression of the coverage with far-field approximation is much less computationally expensive than without the approximations, it can be used for ratios $r_{limit}/l < 0.1$ without compromising too much the accuracy.

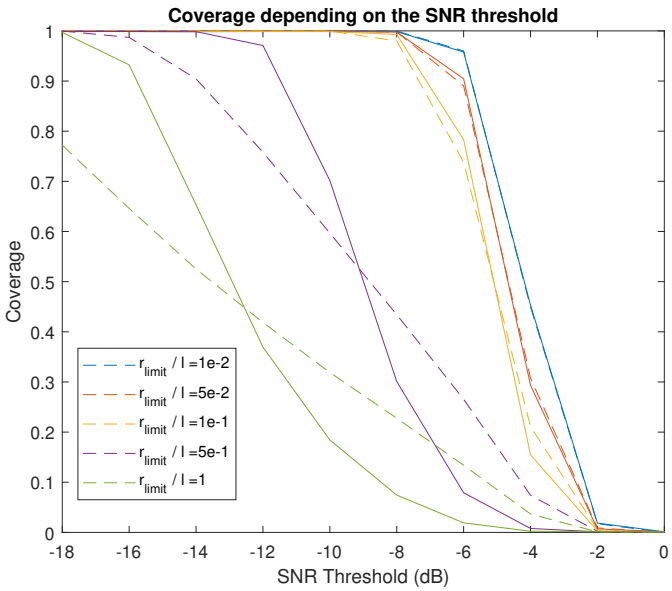

Figure 3.5: Coverage probability for a randomly located RIS, analytically with far-field approximation (plain line) and simulated without far-field approximation (dashed line).

3.3.3 Using a known number of RIS

When using more than one RIS, the assumption will be made that each RIS can be tuned such that the signal received from each RIS is coherent with each others. It is worth noting that the number of RIS's in the network is known, but their location is not known as in the previous development. The expression of the received signal power when using M RIS's made of N elements each then becomes:

$$S = P(|h_q| + |h_c|)^2 \tag{3.28}$$

$$= P\left(|h_q| + \left(\frac{\lambda}{4\pi}\right)\sum_{i=1}^{M}(r_i + d_i)^{-a/2}\sum_{k=1}^{N}\varepsilon_{g,i,k}\varepsilon_{h,i,k}\right)^2 \tag{3.29}$$

When using the hypothesis that d_i, r_i, $\varepsilon_{g,i,k}$ and $\varepsilon_{h,i,k}$ are identically distributed for $i = 1, ..., M$, the CF of $|h_c|$ can be written:

$$\phi_{|h_c|}(\omega) = \mathbb{E}\left[exp(j\omega|h_c|)\right] \tag{3.30}$$

$$= \mathbb{E}\left[exp\left(j\omega\left(\frac{\lambda}{4\pi}\right)\sum_{i=1}^{M}(r_i + d_i)^{-a/2}\sum_{k=1}^{N}\varepsilon_{g,i,k}\varepsilon_{h,i,k}\right)\right] \tag{3.31}$$

$$= \mathbb{E}\left[\prod_{i=1}^{M}\prod_{k=1}^{N}exp\left(j\omega\frac{\lambda}{4\pi}(r_i + d_i)^{-a/2}\varepsilon_{g,i,k}\varepsilon_{h,i,k}\right)\right] \tag{3.32}$$

$$= \prod_{i=1}^{M}\mathbb{E}_{r,\beta}\left[\prod_{k=1}^{N}\mathbb{E}_{\varepsilon_g\varepsilon_h}\left[exp\left(j\omega\frac{\lambda}{4\pi}(r_i + d_i)^{-a/2}\varepsilon_{g,i,k}\varepsilon_{h,i,k}\right)\right]\right] \tag{3.33}$$

$$= \left(\mathbb{E}_{r,\beta}\left[\left(\phi_{\varepsilon_g\varepsilon_h}(j\omega\frac{\lambda}{4\pi}(r + d)^{-a/2})\right)^N\right]\right)^M \tag{3.34}$$

And then when taking into the randomness of r and d and the expression of $\phi_{|h_c|}(\omega)$ found before:

$$\phi_{|h_c|}(\omega) = \left(\int_1^{r_{limit}} \int_{-\pi}^{\pi} \left(\frac{1/\sqrt{\pi}}{(\Gamma(m))^2} G_{2,2}^{2,2} \left[\frac{4}{s^2} \left(\frac{m}{\Omega} \right)^2 \middle| \begin{matrix} 1/2 & 1 \\ m & m \end{matrix} \right] \right)^N \frac{1}{2\pi} \frac{2r}{(r_{limit})^2 - 1} \mathrm{d}\beta \mathrm{d}r \right)^M \quad (3.35)$$

The difference between the effect of the number of elements N and the number of surfaces M is that the RVs r and β are the same for every element, but not for every RIS, which explains the placement of M in the previous expression.

Validation

Similarly as in the previous subsections, expression 3.35 will be validated by comparing the analytic results with the simulation results for two different cases. One with $M = 2$ and the other with with $M = 5$. The other parameters are: $P = 2W$, $\alpha = 4$, $l = 550m$, $BW = 10MHz$, $\lambda = 16.67cm$, $N = 100$,the m-parameter of the Nakagami distribution is $m = 0.5$ and $r_{limit} = 70m$ in order to be able to use the far-field approximation. It should however be noted that the zone where the RIS's are located should be much larger to match real situations, but those cases will be studied at the end of this chapter.
Following figure 3.6, 2 main conclusions can be made. First, as expected increasing the number of RIS's improves well the SNR. Using 2 RIS's allows a coverage of about 100% for SNR threshold of up to $18dB$ and using 5 RIS's allows a coverage of about 100% for an SNR threshold of up to $27dB$. This metric is improved by a ratio of $10^{(6+2.5)/10} \approx 7$ which is higher than $\frac{5}{2}$, this shows that the increasing the spatial diversity of the RIS's has a big impact on the SNR as the high spatial diversity leads to having at least one RIS closer to the UE, which will make the NLoS link stronger than the LoS link. Secondly, an inaccuracy can be observed between the theory and the simulations for values of coverage between 0 and 1, this is probably due to the use of the far-field approximation which showed that for r_{limit}/l ratios above 0.1 (here $\frac{r_{limit}}{l} = \frac{70}{550} \approx 0.13$), there is overestimation by the theory.

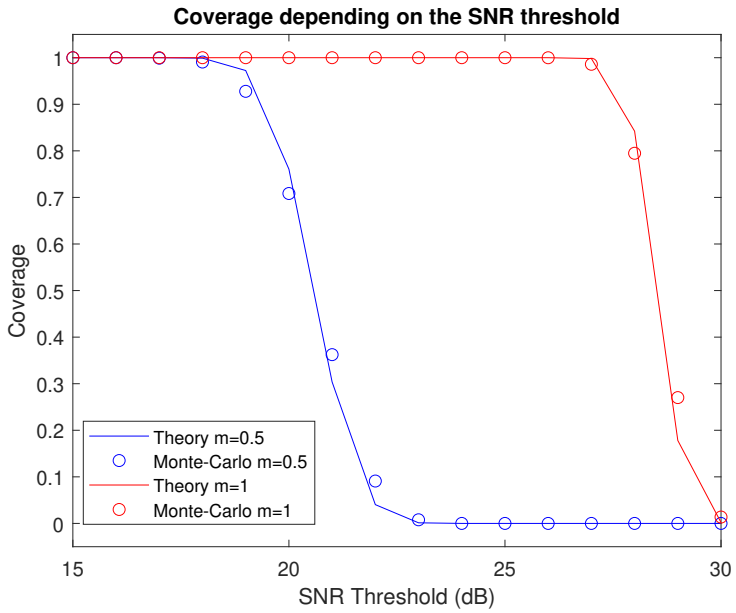

Figure 3.6: Coverage probability for 2 and 5 randomly located RIS

3.3.4 Using a random number of RIS

The final step in this development of the coverage without interference is to model the set of RIS's as a homogeneous Poisson Point Process.
By considering the set of RIS's as being an HPPP, the RIS will still be uniformly distributed across the delimited zone but their number will be random discrete variable following a Poisson distribution of intensity $\lambda_{RIS}|A|$ if A represents the region where the RIS's can be placed.
When taking the zone used until here, A is a 2-dimensional ring centred on the UE, of inner radius 1 and of outer radius r_{limit}, then $|A| = \pi(r_{limit}^2 - 1)$.
To compute the $\phi_{|h_c|}(\omega)$, one can use the property that the CF is the Laplace transform of the pdf of the RV evaluated on $-js$. Then when $F = \sum_{x_i \in \psi_{RIS}} \frac{\lambda}{4\pi}(r_i + d_i)^{-\alpha/2} \sum_{k=1}^{N} \varepsilon_{g,i,k}\varepsilon_{h,i,k} = \sum_{x_i \in \psi_{RIS}} |h_{c,i}|$ and by using the previous relation between the Laplace transform and the PGFL of a HPPP:

$$\begin{aligned} \phi_{|h_c|}(\omega) &= \mathcal{L}_F(-j\omega) && (3.36)\\ &= \mathcal{P}_{\psi_{RIS}} exp(j\omega|h_{c,i}|) && (3.37)\\ &= exp\left[\lambda_{RIS}|A|\left(\phi_{|h_{c,i}|}(\omega) - 1\right)\right] && (3.38) \end{aligned}$$

where $\phi_{|h_{c,i}|}(\omega)$ has the same expression as 3.25 or 3.27, which are the expression of the characteristic function of the NLoS link, either when the far-field approximation is used or not.

Validation

The validation is here conducted with the same set of parameters than in the previous subsection with the exception that here, the density of the PPP of the RIS is specified and not a known number.
When analysing figure 3.7, it is first obvious that the theory predicts well the results of the Monte-Carlo simulation. The conclusion made for the effects on the coverage of increasing the known number of RIS in a network is still valid as the curve for $\lambda_{RIS} = 10^3/km^2$ appears sharper. It is also worth noting that the far-field approximation has been here used, which can lead to some inaccuracies already observed in subsection 3.3.3.

3.4 Coverage Probability with Interference

This section contains the development and the changes from the previous sections to also consider interferences from base stations that are not used by the UE.
The RIS's will still be modelled as an HPPP as it was in the last parts of the previous section.
The interfering BS's will be modelled as a PPP of density λ_{BS} defined on a ring of inner radius l, outer l_{limit} and centred on the UE. The interfering BS's will be limited to a distance l_{limit} from the user, as the assumption could be taken that the power from BS's outside this ring are negligible compared to the AWGN already present.
This section will be composed of 3 different parts:

1. Changes on the coverage expression and on the channel characterization.
2. Computation of the CF of the received interfering power.
3. Numerical results and analysis.

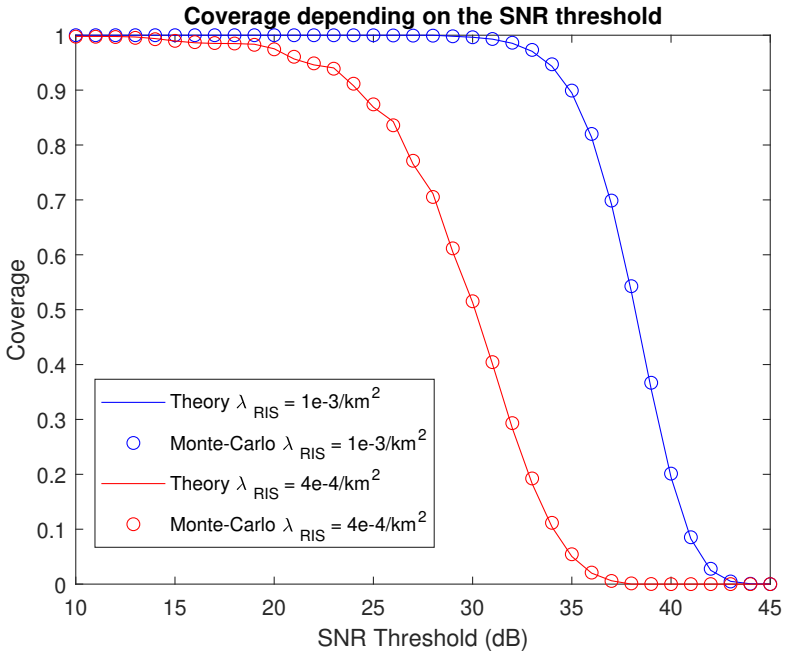

Figure 3.7: Coverage probability for different RIS densities

3.4.1 Channel Characterization

The expression 3.7 of the coverage probability in the previous subsection only included the SNR, now this expression should include the SINR as the interferences are now considered.

$$\mathbb{P}\left[\frac{S}{I+N_0} \leq \theta\right] = \mathbb{P}\left[S - \theta I - \theta N_0 \leq 0\right] \tag{3.39}$$

$$= 1 - F_T(0) \tag{3.40}$$

where $I = \sum_{l_i \in \tilde{\psi}_{BS}} P\frac{\lambda}{4\pi}\varepsilon_i^2 l_i^{-\alpha}$ and $T = S - \theta I - \theta N_0$. The Gil-Pelaez inversion law will again be used to compute F_T. The CF $\phi_T(\omega)$ is thus needed, the CF of the addition of two different RV has already been given as being the product of the CF of both RV, which results for T:

$$\phi_T(\omega) = \phi_S(\omega)\phi_{-\theta I}(\omega)\phi_{-\theta N_0}(\omega) \tag{3.41}$$

However by applying the definition of the CF on $\phi_{-\theta I}(\omega)$ and $\phi_{-\theta N_0}(\omega)$, and using the fact that N_0 and θ are not random:

$$\phi_{-\theta I}(\omega) = \mathbb{E}\left[exp\left(-j\omega\theta I\right)\right] \tag{3.42}$$

$$= \phi_I(-\theta\omega) \tag{3.43}$$

$$\phi_{-\theta N_0}(\omega) = exp\left(-j\theta N_0\right) \tag{3.44}$$

The first step to compute the expression 3.41, is to compute $\phi_S(\omega)$. In the previous section S, the received signal power, was defined as $P(|h_q| + |h_c|)^2$ by considering that the LoS and the NLoS link were coherent. However, as now the distribution of S is needed in the coverage probability and not only the distribution of $|h_c| + |h_q|$, one should now derive the distribution of $(|h_q| + |h_c|)^2$, which is impossible considering the distribution of $|h_q|$ and $|h_c|$.

The assumption will here be taken that the LoS link and the NLoS are fully non-coherent and thus, $S = P(|h_q|^2 + |h_c|^2)$. This assumption will be compared to Monte Carlo simulations where the signals are coherent in the validation part.
First, let us compute the CF of $|h_q|^2$. A squared random variable Nakagami-m distributed with parameters m and mean fading power Ω follows a gamma distribution of shape parameter m and of scale parameter Ω/m. As $|h_q|^2 = \left(\frac{\lambda}{4\pi}\right)^2 \varepsilon_q^2 l^{-\alpha}$, the CF of $|h_q|^2$ is defined by:

$$\begin{aligned} \phi_{|h_q|^2}(\omega) &= \phi_{\varepsilon_q^2}\left(\left(\frac{\lambda}{4\pi}\right)^2 l^{-\alpha}\omega\right) && (3.45) \\ &= \left(1 - j\frac{\Omega\left(\frac{\lambda}{4\pi}\right)^2 \omega}{m l^{\alpha}}\right)^m && (3.46) \end{aligned}$$

To compute the CF of $|h_c|^2$, it is not possible to still consider that $|h_c|$ follows the distribution of a product of two Nakagami-m RV as it would not be possible to compute the distribution of $|h_c|^2$. Nevertheless knowing that for each RIS $|h_c|$ is related to the sum of products of Nakagami-m distributed RV as it can be seen in the equation 3.2 , it is possible to apply the central limit theorem (CLT) to $|h_c|$ as it is suggested in [12]. The central limit theorem is stated at appendix 2.2.1.
From [12], for large values of N, the distribution of $|h_c|$ can be approximated by:

$$\begin{aligned} |h_c| &\sim \mathcal{N}\left(N\frac{\lambda}{4\pi}(r+d)^{-\alpha/2}\mathbb{E}\left[\varepsilon_g\varepsilon_h\right], N\left(\frac{\lambda}{4\pi}\right)^2 (r+d)^{-\alpha} Var\left[\varepsilon_g\varepsilon_h\right]\right) && (3.47) \\ \text{where: } \mathbb{E}\left[\varepsilon_g\varepsilon_h\right] &= \left(\frac{\Gamma\left[m+1/2\right]}{\Gamma\left[m\right]}\right)^2 \frac{\Omega}{m} && (3.48) \\ Var\left[\varepsilon_g\varepsilon_h\right] &= \left(\frac{\Gamma\left[m+1\right]}{\Gamma\left[m\right]}\frac{\Omega}{m}\right)^2 - \mathbb{E}\left[\varepsilon_g\varepsilon_h\right]^2 && (3.49) \end{aligned}$$

This approximation will be more and more accurate where N becomes larger, the accuracy of this approximation depending on N is checked on appendix A.
Also, if $X \sim \mathcal{N}\left(\mu, \sigma^2\right)$, the distribution of X^2 is related to the non-central chi-squared distribution:

$$\frac{X^2}{\sigma^2} \sim \chi^2(1, \frac{\mu^2}{\sigma^2}) \tag{3.50}$$

By using this last property and the normal approximation of $|h_c|$, the CF of a non-central chi-squared distribution can be used to compute the CF of $|h_c|^2$:

$$\begin{aligned} \phi_{|h_c|^2}(\omega) &= \phi_{|h_c|^2/\sigma^2}(\omega\sigma^2) && (3.51) \\ &= exp(\frac{j\mu^2\omega}{1-2j\sigma^2\omega})(1-2j\sigma^2\omega)^{-1/2} && (3.52) \end{aligned}$$

For $\mu = N\frac{\lambda}{4\pi}(r+d)^{-\alpha/2}\mathbb{E}\left[\varepsilon_g\varepsilon_h\right]$ and $\sigma^2 = N\left(\frac{\lambda}{4\pi}\right)^2 (r+d)^{-\alpha} Var\left[\varepsilon_g\varepsilon_h\right]$. Knowing $\phi_{|h_q|^2}(\omega)$ and $\phi_{|h_c|^2}(\omega)$, the CF of S can be computed as: $\phi_S(\omega) = \phi_{|h_q|^2}(P\omega)\phi_{|h_c|^2}(P\omega)$.

3.4.2 The Characteristic Function of the Interfering Power

As already mentioned in the previous section, the power of interference is expressed by $I = \sum_{l_i \in \tilde{\psi}_{BS}} P\frac{\lambda}{4\pi}\varepsilon_i^2 l_i^{-\alpha}$.
Where ε_i is Nakagami-m distributed with parameter m and mean fading power Ω and thus ε_i^2 follows

a gamma distribution of shape parameter m and of scale parameter Ω/m. The interferences are here modelled as following a LoS link as it has been shown in [32], [16], [14], [29] and [18] that the RIS have more influence on the signal than on the interferences.
The CF of I can be computed in a similar way to [5] by using the relation between the Laplace transform and the characteristic function and then using the PGFL of a Poisson Point Process. The expression of the CF of I is:

$$\phi_I(\omega) = exp\left\{\pi\lambda_{BS}\left[{}_2F_1(m, \frac{-2}{\alpha}, 1-\frac{-2}{\alpha}, \frac{j\omega P\Omega\lambda^2}{ml^\alpha 16\pi^2})l^2\right]_l^{l_{limit}}\right\} \tag{3.53}$$

The proof of this expression is available in the appendix B.
Now that all the characteristic functions are computed, the outage probability can be written by using the Gil-Pelaez inversion law:

$$\begin{aligned}\mathbb{P}\left[\frac{S}{I+N_0} \leq \theta\right] &= \mathbb{P}\left[S - \theta I - \theta N_0 \leq 0\right] && (3.54)\\ &= 1 - F_T(0) && (3.55)\\ &= 1 - \frac{1}{2} + \frac{1}{\pi}\int_0^\infty Im\left(exp(j0\omega)\phi_S(\omega)\phi_I(-\theta\omega)exp(-j\theta N_0)\right)\omega^{-1}\mathrm{d}\omega && (3.56)\end{aligned}$$

Validation

The accuracy of the previous development will be checked when 3 different variables change, the BS's density λ_{BS}, the maximal distance of an interfering BS l_{limit} which both influence the interfering power and the density of RIS's λ_{RIS}.
For the 3 experiments, the common variable were $P = 2W$, $l = 600m$, $r_{limit} = 600$, $\alpha = 4$ $f = 1.8GHz$, $BW = 10MHz$, $N = 100$ and $m = 1$ for the Nakagami-distributed fading. It should also be noted that the far-field approximation is not used here.
On figure 3.8, the coverage probability for $\lambda_{RIS} = 100/km^2$, $l_{limit} = 4000$ and varying λ_{BS} is displayed. There are obvious differences between the theory and the simulations and as expected, increasing the density of BS's decreases the SINR and therefore impairs the coverage probability.
On figure 3.9, two different value for the limit of the interfering BS zone l_{limit} are tested. First, the theory follows well the simulation, therefore the theory takes well into account the impact of the interferences. As expected, increasing the zone while keeping the same BS's density $\lambda_{BS} = 100/km^2$ worsens well the SINR, however the difference is not very important in term of coverage probability. This can be explained by the fact that the majority of the interfering power comes from BS's that are almost as close to the UE than the used BS (here $l = 600m$). Taking into account an even larger zone should therefore to have a big impact on the SINR.
On figure 3.10, different density of RIS are tested. As already observed in the case without interference, increasing the density of RIS leads to a large improvement in the coverage. It is also to be noted that the theory predicts accurately the simulation results, but the simulation uses the case where the LoS and NLoS link are non-coherent ($S = P(|h_c|^2 + |h_q|^2)$) which is a lower bound for the signal power compared to any other phase shift between the LoS and NLoS link. On figure 3.11, the theory with non-coherent link is compared with simulation results where both links are coherently added. It is obvious that the non-coherent is a lower bound and this bound seems to be further from the upper bound (the coherent case)when density of RIS increases.

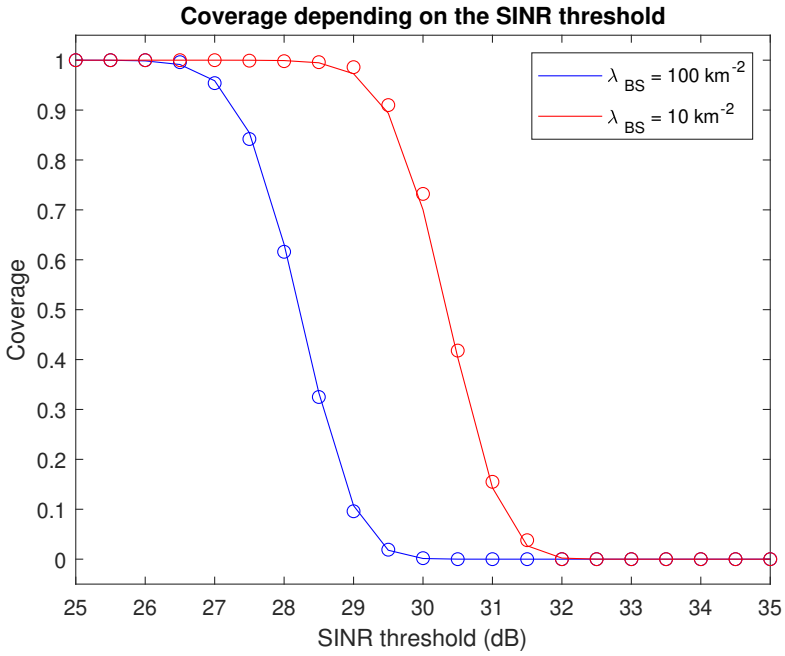

Figure 3.8: Coverage probability for different BS densities

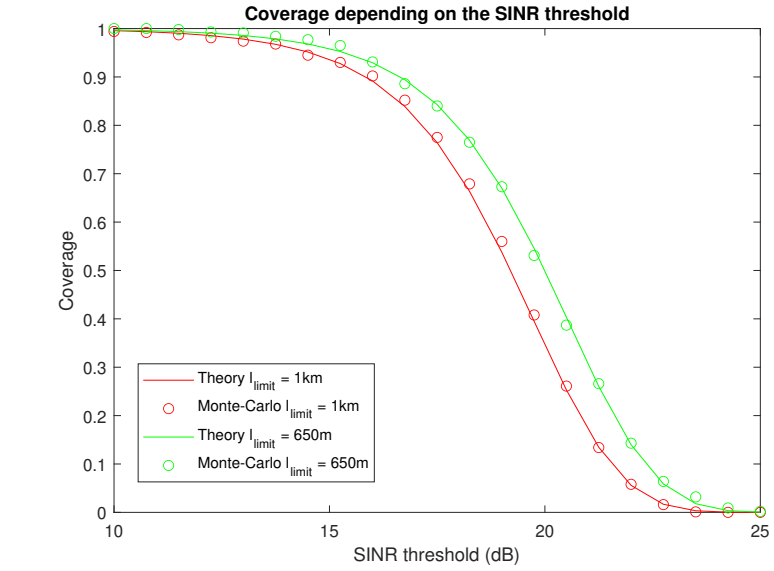

Figure 3.9: Coverage probability for different BS zone limits

3.5 Numerical results and analysis

In this section different experiments will be presented and analysed in order to quantify the improvement brought by the RIS's in different situations.

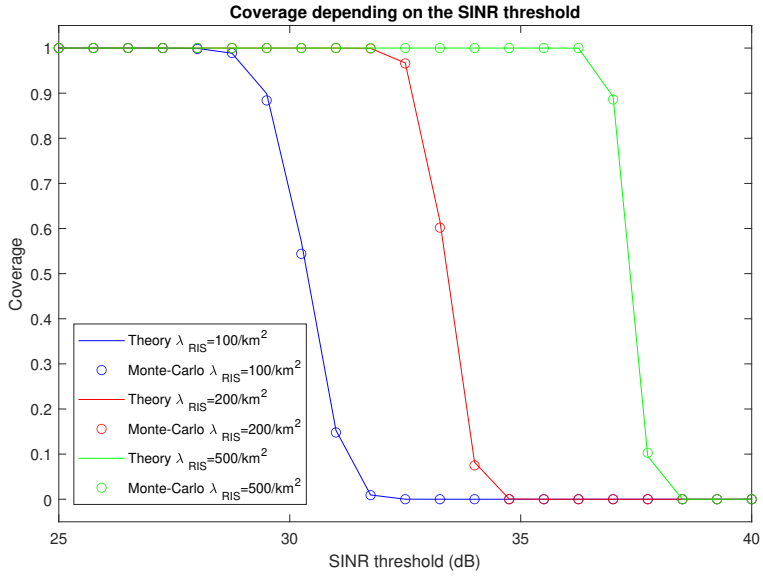

Figure 3.10: Coverage probability for different RIS densities

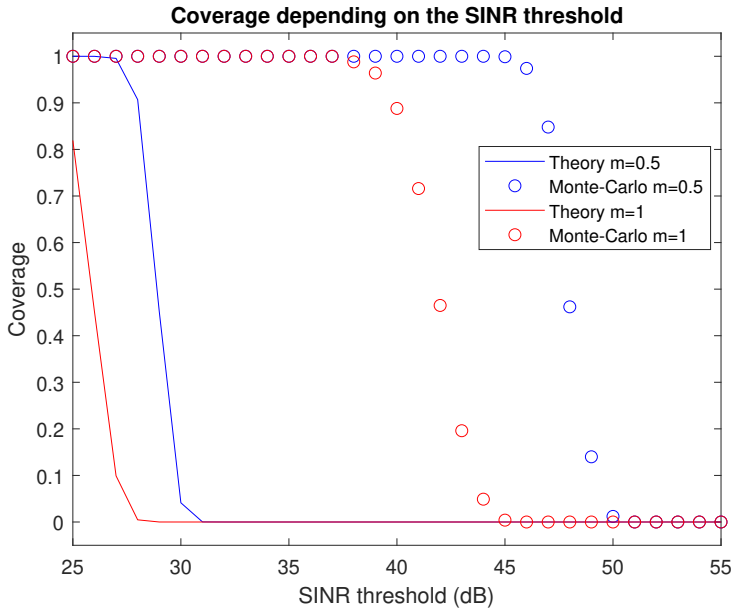

Figure 3.11: Coverage probability for different RIS densities, with coherent links simulation

3.5.1 Improvement when using RIS compared to the LoS link

In order to justify the use of the RIS's, the coverage of the network will be compared for different values of density of RIS or when totally removing the NLoS link. r_{limit} has been here set to be equal to l, the distance UE-BS as using an RIS further than the BS would be (without blockages) an unrealistic scenario.
On figure 3.12, the increase of coverage brought by the RIS's is evident, even for $\lambda_{RIS} = 1/km^2$ where there is only in average 1.13 RIS in circular zone of $600m$ of radius, the performance of the RIS-aided network are much better than the network only using the LoS link.

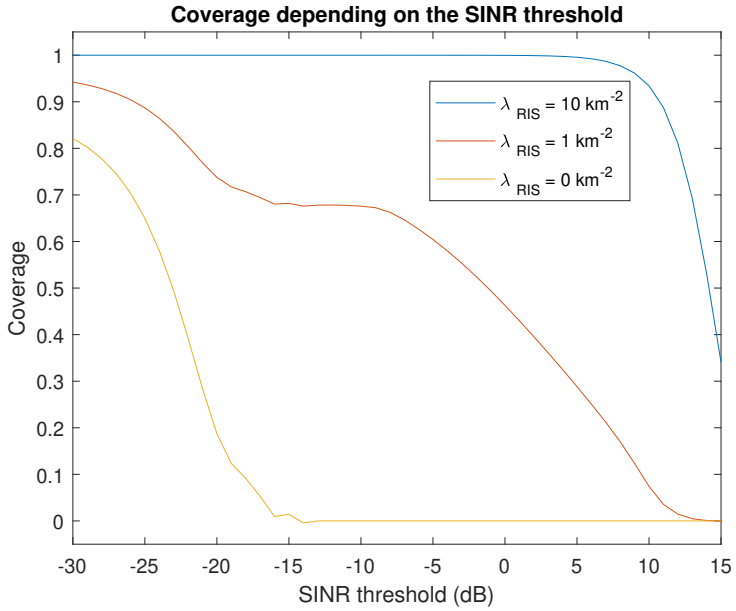

Figure 3.12: Coverage for scenario without RIS or with different values of RIS density

An interesting thing to observe for $\lambda_{RIS} = 1/km^2$ is that there is a stable region at about 70% of coverage probability. This region comes from the non-negligible probability in this case that no RIS is present in the network, which effectively becomes a LoS only wireless network. This stable region is not present for $\lambda_{RIS} = 10/km^2$ as the probability of having no RIS in the network is way lower.

3.5.2 Number of RIS to use

When placing the RIS in a wireless network, the two parameters that can be changed are N the number of elements per surface and λ_{RIS} the density of RIS within the RIS zone. Multiple sets of those parameters totalling the same number of total elements (with all RIS added) will be tested:

Number of elements	RIS density (km^{-2})
50	1000
100	500
200	250
500	100

Table 3.1: Set of parameters tested to compare the density of RIS and the number of elements

The result of the coverage for those sets of parameters is available on figure 3.13. The coverage is improved when N increases. This mostly comes from the path loss used to model the reflection on the RIS. When $|h_c| = \left(\frac{\lambda}{4\pi}\right)(r+d)^{-a/2}\sum_{k=1}^{N}\varepsilon_g\varepsilon_k$ is used, increasing N has a direct impact on $|h_c|$ and multiplying N by k will result in a signal power multiplied by k. Decreasing λ_{RIS} will also decrease the number of RIS very close to the UE. However, with this signal propagation model, the impact of an increase of r is very limited.

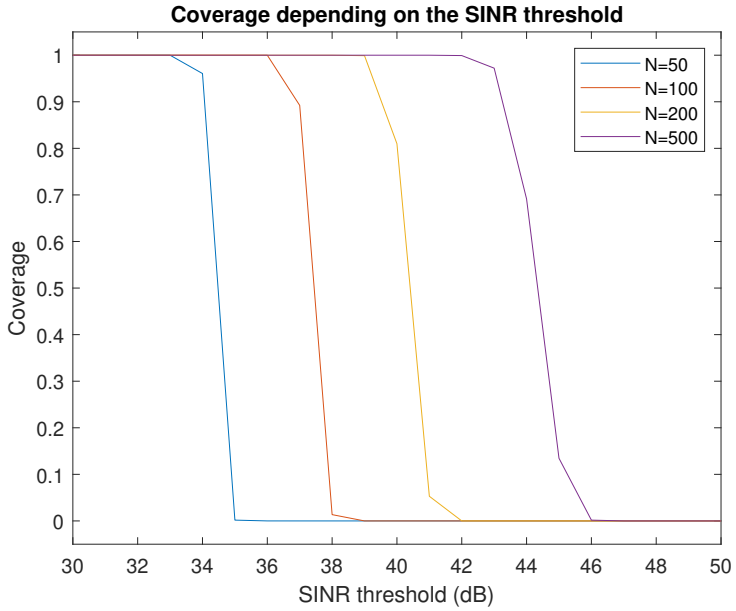

Figure 3.13: Comparison of the trade-off between the number of elements and the density of RIS

3.5.3 Size of the zone with RIS

When establishing a link between the UE and the BS, the size of the disk inside of which the RIS's are located should be limited for two main: the first being that in a more realist scenario, other UEs are also present and therefore all the RIS should not be allocated to only one UE, also because of the path-loss, the RIS located beyond a given distance of the UE will only reflect signal whose power signal will be negligible compared to the LoS link power.
That is why it is relevant to compare different size of the zone with RIS, and therefore different r_{limit} to check whether for certain values of r_{limit}, the enlargement of the RIS-zone still improve the coverage in a non-negligible way.
The experiment on figure 3.14 has been for a network where the distance UE-BS is $1km$ and the density of RIS is $\lambda_{RIS} = 100km^{-2}$. By looking at 3.14, it is clear that the enhancement of coverage is more important when changing r_{limit} from $400m$ to $600m$ than when changing r_{limit} from $600m$ to $800m$. Even though the first change adds in average $10^{-4}\pi(600^2 - 400^2) = 62.8$ possible RIS's in the network and the second change adds in average $10^{-4}\pi(800^2 - 600^2) = 88.0$ possible RIS's in the network.
This highlights the fact that beyond a given distance from the UE, the RIS's will generally not improve the coverage that much and that the location of the RIS is as much important than the density or their number or elements in order to provide link that can provide a better SNR than the LoS link.

3.6 Chapter Summary

In this chapter, the enhancement of coverage from the use of RIS's has been highlighted. In a situation with no blockage, the SINR threshold can be increased by tens of dB while having the same coverage probability. As no limits are modelled on the density of RIS or the number of elements N, this enhancement can theoretically be infinite, as the coverage probability increases when the RIS network is more dense and each RIS is build with more elements.
However, the assumption of having non-coherent links in theory leads to a non-negligible underestimation of the coverage as shown on figure 3.11.

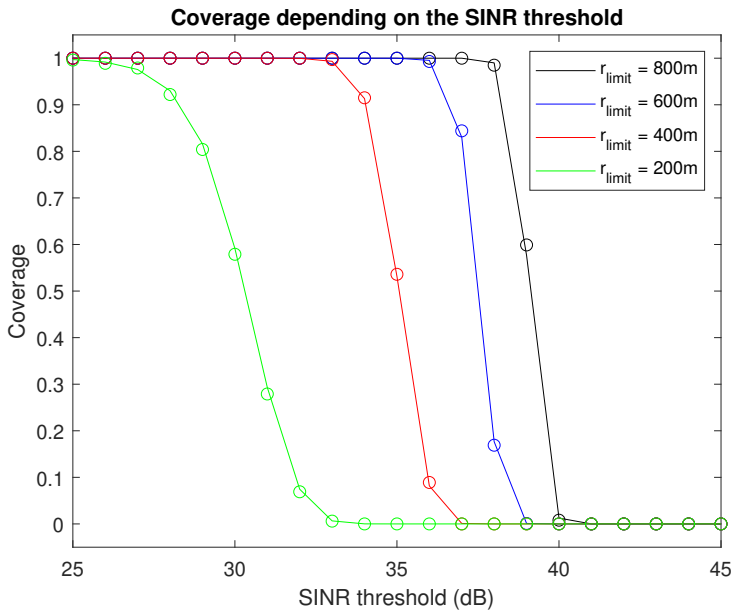

Figure 3.14: Comparison of different sizes of RIS-zone

With this path-loss model, it has also been shown that a few large RIS's (with a lot of elements) are more efficient than a lot of smaller RIS's.
Finally it has been shown that to be efficient, the RIS's should be located be located close to the UE and that there exists a limit on the size in which the RIS's can be used to efficiently enhance the coverage.

Chapter 4

Association rules for RIS-aided wireless networks impaired by blockages

4.1 Introduction

This chapter aims at modelling a RIS-aided wireless network with the presence of obstacles and comparing the performances of different association rules. Like in the previous chapter, the network is impaired by interferences, is impact by a Nakagami-m distributed small-scale fading gains and the same propagation model is used for the RIS.

4.2 System Model

4.2.1 Geometric description of the network

In this model, a UE will try to reach an available BS in the network. The network contains multiple BS's, these BS's are modelled by a PPP of density λ_{BS} and located inside a disk of radius l_{limit}. To reach the BS, the UE could use at most one RIS at a time, these RIS's are modelled by a PPP of density λ_{RIS} and are located inside a disk of radius r_{limit}. The RIS that will be used among the available RIS's is the one which minimizes the distance $(r + d)$, the distance UE-RIS-BS. The definition of "availability" will be found at the end of this section.
The difference between this model and the model used in the previous model is that this network contains obstacles. From [15], these obstacles are modelled as a line segment of length L and angle θ. The mid-point of those line segment is modelled by a PPP of density λ_{Obs} inside a disk of radius l_{limit}. The assumption will be taken that the RIS will be installed on obstacles such as walls of building. Thus, $\lambda_{Obs} > \lambda_{RIS}$ as there can't be more obstacles than RIS.
The signal power S when using the BS of index k is here defined by:

$$S = P(|h_q|^2 + |h_c|^2) \tag{4.1}$$

$$= P\left(\frac{\lambda}{4\pi}\right)^2 \left(\varepsilon_q^2 l_k^{-\alpha}\delta_{L,k} + (r_k + d_k)^{-\alpha}\left(\sum_{i=1}^{N}\varepsilon_{g,i}\varepsilon_{h,i}\right)^2 \delta_{R,k}\right) \tag{4.2}$$

where P is the transmit power, $|h_q|$ is the channel gain of the LoS link, $|h_c|$ the channel gain of the NLoS link, l_k the distance between the UE and the k^{th} closest RIS, r_k is the distance between the UE and the RIS, d_k the distance RIS-BS, ε_q the Nakagami-m distributed channel small-scale fading gain of the LoS link, $\varepsilon_{g,i}$ the Nakagami-m distributed channel small-scale fading gain of the link between the UE and the i^{th} element of the RIS and $\varepsilon_{h,i}$ the Nakagami-m distributed channel small-scale fading gain of the link between the i^{th} element of the RIS.

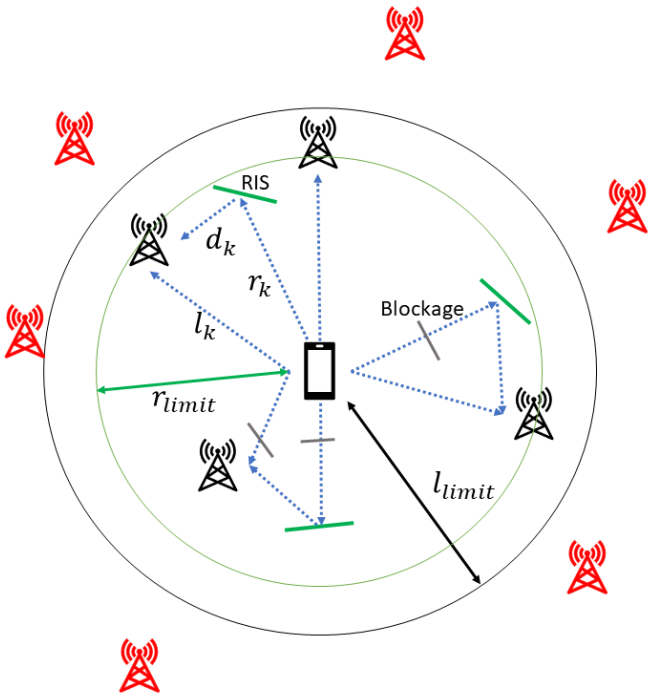

Figure 4.1: System Model Scheme

Finally the factors $\delta_{L,k}$ and $\delta_{R,k}$ model the blockage on each link. In [2], it has been derived that the probability that a LoS link is not blocked is $exp\left(-\frac{2\lambda_{Obs}\mathbb{E}[L]l_k}{\pi}\right)$, where $\mathbb{E}[L]$ is the average length of an obstacle. To model the blockage of the LoS link, $\delta_{L,k}$ will be equal to 1 with a probability $exp\left(-\frac{2\lambda_{Obs}\mathbb{E}[L]l_k}{\pi}\right)$ and to 0 otherwise.
To be available for reaching the BS, the RIS has to satisfy the 4 following criteria [15]:

1. The link UE-RIS must not be blocked. This condition is satisfied with a probability of $exp\left(\frac{-2\lambda_{Obs}\mathbb{E}[L]r_k}{\pi}\right)$.
2. The link RIS-BS must not be blocked. This condition is satisfied with a probability of $exp\left(\frac{-2\lambda_{Obs}\mathbb{E}[L]d_k}{\pi}\right)$.
3. Both the incident wave and the reflected wave should be located on the same side of the RIS. The probability that this condition is satisfied is : $1-\frac{1}{\pi}\arccos\left(\frac{r_k-l_l cos(\beta)}{r_k^2+l_k^2-2r_k l_k cos(\beta)}\right)$. The proof is available in [15].
4. The reflecting side of the RIS should be on the side facing the UE and the BS. This condition is fulfilled with a probability $\frac{1}{2}$.

The coefficient $\delta_{R,k}$ will be equal to 1 if there is at least one RIS available, otherwise $\delta_{R,k}=0$.

4.2.2 Association rules

Different ways of reaching a BS in a network including RIS and blockages will be compared to see if there is an optimal way of using the RIS. Some of those association rules can be theoretically modelled, otherwise a Monte-Carlo is used to compute the results of coverage. The different association rules are:

1. Attempting to reach the closest BS possible by using a LoS link, a NLoS link (with the help of an RIS) or the combination of both. This is the base rule used for the theoretical computations done in the next section.
2. Removing the RIS of the system and reaching the closest BS available using only a LoS link. This rule can be theoretically modelled.
3. Prioritizing the use of a LoS link. The UE will first try to reach the BS inside the a disk of radius l_{limit} only with a LoS link then the UE will try to use the RIS. This rule can be theoretically modelled.
4. Attempting to reach the closest BS possible by using a LoS link or a NLoS link but the combination of both is excluded. In case if both links are available, only the LoS link will be used. This rule can be theoretically modelled.
5. Analysing the entire network of BS and RIS, and selecting the BS which will maximized the received SINR. This rule will only be applied using simulations where each possible combinations of RIS and BS will be tested to choose the one resulting in the best SINR possible.

4.3 Coverage Probability

To model the coverage probability of this system, 6 random variables need to be taken account of, these are:

- The random small scale fading gains that impact the different links.
- The type of link used to reach the BS (LoS, NLoS or both).
- The distance between the UE and the BS.
- The index of the used BS.
- The distance between the UE and the RIS.
- The angle BS-UE-RIS.

These random variables will be included progressively in the coverage probability calculations.

4.3.1 Random fading gain

Let S be the power of signal transmitted, I the power of interference, N_0 the power of the white noise and θ the SNR threshold of the receiver. Then the outage probability can be written as:

$$\mathbb{P}\left(\frac{S}{I+N_0} < \theta\right) \quad = \quad \mathbb{P}\left(S - \theta I - \theta N_0 < 0\right) \tag{4.3}$$

Then using the Gil-Pelaez inversion theorem to use the characteristic function of S, I and N_0 to derive the cdf of $\frac{S}{I+N_0}$.

$$\mathbb{P}\left(S - \theta I - \theta N_0 < 0\right) \quad = \quad \frac{1}{2} - \frac{1}{\pi}\int_0^\infty Im\left(\phi_S(\omega)\phi_I(-\theta\omega)exp(-jN_0\theta\omega)\right)\omega^{-1}d\omega \tag{4.4}$$

The interference will only be taken into account as following a line of sight path like in the previous chapter. The equation 3.53 can thus be reused.
The power of the signal S will be different on the path used: line of sight, through the reflection of an RIS or both paths, its characteristic function should be derived for every case.

4.3.2 The different types of link

To take into account the different links possible, one should take the expected value of the outage probability in function of the path used. The different options of paths will be represented by the discrete random variable M:

$$\begin{aligned}
\mathbb{P}\left(S-\theta(I+N_0)<0\right) &= \mathbb{E}_M\left[\frac{1}{2}-\frac{1}{\pi}\int_0^\infty Im\left(\phi_{S,m}(\omega)\phi_I(-\theta\omega)exp(-jN_0\theta\omega)\right)\omega^{-1}d\omega\right] &(4.5)\\
&= \frac{1}{2}-\frac{1}{\pi}\int_0^\infty Im\left(\mathbb{E}_M\left[\phi_{S,m}(\omega)\right]\phi_I(-\theta\omega)exp(-jN_0\theta\omega)\right)\omega^{-1}d\omega &(4.6)\\
\text{where : } \mathbb{E}_M\left[\phi_{S,m}(\omega)\right] &= \sum_{m=1}^{3}\phi_{S,m}(\omega)p_M(m) &(4.7)
\end{aligned}$$

$p_M(m)$ being the probability mass function (pmf) of the random variable describing the type of link used.

1. In a case where only a line of sight path is used for the signal, then $S=P\frac{\lambda^2}{16\pi^2}|\varepsilon_q|^2 l^{-\alpha}$ where ε_q is Nakagami-m distributed with a mean fading power of Ω and an m-parameter m, l_k being the UE-BS distance

   As previously demonstrated:

$$\begin{aligned}
\phi_{S,1}(\omega) &= \phi_{|\epsilon_q|^2}(j(\omega P l_k^{-\alpha})) &(4.8)\\
&= \left(1-j\frac{\Omega\omega P}{m l_k^\alpha}\frac{\lambda^2}{16\pi^2}\right)^{-m} &(4.9)
\end{aligned}$$

2. In a case where only the reflected wave from one RIS with N elements is used for the signal, then:

$$\begin{aligned}
S &= P\frac{\lambda^2}{16\pi^2}(d+r)^{-\alpha}(\sum_{i=1}^{N}\epsilon_{g,i}\epsilon_{h,i})^2 &(4.10)\\
&= P|h_c|^2 &(4.11)
\end{aligned}$$

   Using a similar development than for 4.12, but for only one RIS used, the characteristic function of S is obtained:

$$\phi_{S,2}(\omega) = exp(\frac{j\mu^2\omega}{1-2j\sigma^2\omega})(1-2j\sigma^2\omega)^{-1/2} \quad (4.12)$$

   For $\mu = N\frac{\lambda}{4\pi}(r+d)^{-\alpha/2}\mathbb{E}\left[\varepsilon_g\varepsilon_h\right]$ and $\sigma^2 = N\left(\frac{\lambda}{4\pi}\right)^2(r+d)^{-\alpha}Var\left[\varepsilon_g\varepsilon_h\right]$.

3. When both links are used, then the power of the signal is written:

$$S = P\frac{\lambda^2}{16\pi^2}|\epsilon_q|^2 l^{-\alpha} + P\frac{\lambda^2}{16\pi^2}(d+r)^{-\alpha}\sum_{i=1}^{N}\epsilon_{g,i}\epsilon_{h,i} \quad (4.13)$$

   Then when considering that the fading gains of both links are independent:

$$\phi_{S,3}(\omega) = \phi_{S,1}(\omega)\phi_{S,2}(\omega) \quad (4.14)$$

Let us now compute $p_M(m)$, it is first worth noticing that $p_M(1) \cup p_M(2) \cup p_M(3)$ is the probability that a link exists, which can be written as $1-(1-P_{LOS}(l_k))(1-P_{RIS}(l_k))$ with $P_{LOS}(l_k)$ being the probability that a LoS link exists between the UE and a BS at a distance l_k. $P_{RIS}(l_k)$ is the probability that a link going by a RIS exists between the UE and a BS at a distance l_k from each other. $p_M(m)$ will then be defined as:

$$p_M(m)(1-(1-P_{LOS}(l_k))(1-P_{RIS}(l_k))) = \begin{cases} P_{LOS}(l_k)(1-P_{RIS}(l_k) & \text{for m=1} \\ (1-P_{LOS}(l_k))P_{RIS}(l_k) & \text{for m=2} \\ P_{LOS}(l_k)P_{RIS}(l_k) & \text{for m=3} \end{cases} \quad (4.15)$$

The expression of $P_{LOS}(l)$ and $P_{RIS}(l,r)$ have been computed in [15]:

$$P_{LOS}(l) = exp\left(-\frac{2\lambda_{Obs}\mathbb{E}[L]}{\pi}l\right) \quad (4.16)$$

$$P_{RIS}(l) = 1-exp\Bigg(-\lambda_{RIS}\int_{-\pi}^{\pi}\int_{0}^{\infty}\frac{1}{2}P_{LOS}(r)P_{LOS}(\sqrt{l^2+r^2-2rlcos(\beta)}) (1-\frac{1}{\pi}\arccos\frac{r-l\cos(\phi)}{\sqrt{r^2+l^2-2rlcos(\beta)}})r\mathrm{d}r\mathrm{d}\phi\Bigg) \quad (4.17)$$

4.3.3 The distance between the UE and the BS

The distance l_k between the UE and the BS index k (the one used to transmit signal) is also random and the outage probability should also be averaged over l_k. It is worth noting that the interference also depends on l_k. It should therefore also be averaged on l_k:

$$\mathbb{P}(S-\theta I-\theta N_0<0) = \mathbb{E}_{L_k}\mathbb{E}_M\left[\frac{1}{2}-\frac{1}{\pi}\int_0^{\infty}Im\left(\phi_{S,m}(\omega)\phi_I(-\theta\omega)exp(-jN_0\theta\omega)\right)\omega^{-1}d\omega\right] \quad (4.18)$$

$$= \frac{1}{2}-\frac{1}{\pi}\int_0^{\infty}Im\left(\mathbb{E}_{L_k}\mathbb{E}_m\left[\phi_{S,m,k}(\omega)\right]\phi_I(-\theta\omega)exp(-jN_0\theta\omega)\right)\omega^{-1}d\omega \quad (4.19)$$

$$= \frac{1}{2}-\frac{1}{\pi}\int_0^{\infty}Im\Bigg[\left(\int_0^{\infty}\left(\sum_{m=1}^{3}\phi_{S,m}(\omega,k)p_M(m,k)\right)\phi_I(-\theta\omega)f_{L_k}(l_k)\mathrm{d}l_k\right) exp(-jN_0\theta\omega)\Bigg]\omega^{-1}d\omega \quad (4.20)$$

$f_{L_k}(l_k)$ represents the probability distribution function of the distance between the UE and the kth base station. When modelling as a homogeneous Poisson Point Process, this probability can be modelled as the probability that the k^{th} neighbour is located at a distance l_k. With λ_{BS} being the density of the Poisson Point Process for the base stations, this expression is found in [19] :

$$f_{L_k}(l_k) = \frac{2(\lambda_{BS}\pi)^k(l)^{2k-1}exp(-\lambda_{BS}\pi l_k^2)}{k!} \quad (4.21)$$

It is worth noting that in a real case, after a given distance l_{limit} the received signal becomes almost negligible as it is divided, therefore the upper bound of the integral over l can be changed as:

$$\mathbb{P}(S-\theta I-\theta N_0<0) = \frac{1}{2}-\frac{1}{\pi}\int_0^{\infty}Im(\left(\int_0^{l_{limit}}\left(\sum_{m=1}^{3}\phi_{S,m}(\omega,k)p_M(m,k)\right)\phi_I(-\theta\omega)f_{L_k}(l_k)\mathrm{d}l_k\right) exp(-jN_0\theta\omega))\omega^{-1}d\omega \quad (4.22)$$

Approximation 1

In reality the distance UE-BS cannot modelled by using an HPPP ψ_{BS} for the BS. The BS that are reachable are either the one whose LoS link is not blocked or for which an unblocked NLoS link exist. Those two conditions can be modelled as a thinning of ψ_{BS} which yields an IPPP . However the distance from the UE to the k^{th} closest neighbour can generally not be computed for an IPPP.
The reachable BS is thus modelled as an HPPP to compute $f_{L_k}(l_k)$ and the expression 4.21 will be used, this approximation leads to an inaccuracy on the distance between the UE and the k^{th} closest BS.

4.3.4 Different Base Station

In those expressions the index of the chosen base station can be different depending on the chosen association rule, it is thus also a random variable. The expected value of the outage probability depending on the index k of the base station should also be taken.

$$\begin{aligned}
\mathbb{P}\left(\frac{S}{I+N_0}<\theta\right) &= \mathbb{E}_{K,L_k,M}\left[\frac{1}{2}-\frac{1}{\pi}\int_0^\infty Im\Big[\phi_{S,m}(\omega)\phi_I(-\theta\omega)exp(-jN_0\theta\omega)\Big]\omega^{-1}d\omega\right] &(4.23)\\
&= \frac{1}{2}-\frac{1}{\pi}\int_0^\infty Im\Big[\mathbb{E}_{K,L_k,M}\left[\phi_{S,m}(\omega)\right]\phi_I(-\theta\omega)exp(-jN_0\theta\omega)\Big]\omega^{-1}d\omega &(4.24)\\
&= \frac{1}{2}-\frac{1}{\pi}\int_0^\infty Im\Bigg[\Bigg(\sum_{k=1}^{N_{BS}}\Bigg(\int_0^{l_{limit}}\left(\sum_{m=1}^{3}\phi_{S,m}(\omega,k)p_M(m,k)\right)\phi_I(-\theta\omega)\\
&\quad f_{L_k}(l_k)\mathrm{d}l_k\Bigg)p_K(k)\Bigg)exp(-jN_0\theta\omega)\Bigg]\omega^{-1}d\omega &(4.25)
\end{aligned}$$

The functions $\phi_{S,M}(\omega,k)$ and $p_M(m,k)$ will only depend on k through the variable l_k, which is already a random variable whose pdf varies on k. There are thus no need to modify those functions for now.
The pmf of k will depend on the association rule used, the first rule is used here, which is to take the closest base station that can be reached either by a line of sight or an indirect link.

$$p_K(k) = \begin{cases} 1-(1-P_{L1})(1-P_{I1}) & \text{if } k=1\\ (1-(1-P_{Lk})(1-P_{Ik}))\prod_{i=1}^{k-1}(1-P_{Li})(1-P_{Ii}) & \text{if } 1<k\leq N_{BS}\\ \prod_{i=1}^{N}(1-P_{Li})(1-P_{Ii}) & \text{if } k=N_{BS}+1\text{, no BS can be reached}\end{cases} \quad (4.26)$$

where P_{Lk} (P_{Ik}) represents the probability that kth base station is reachable by a LoS (NLoS) link. This can be expressed as the expected value of $P_{LOS}(l_k)$ ($P_{RIS}(l_k)$) with l_k being the distance between the UE and the kth BS. Then:

$$P_{Lk} = \int_0^\infty P_{LOS}(l_k)f_{L_k}(l_k)\mathrm{d}l_k \quad (4.27)$$

$$P_{Ik} = \int_0^\infty P_{RIS}(l_k)f_{L_k}(l_k)\mathrm{d}l_k \quad (4.28)$$

Finally, it is useful to ensure that $\sum_{k=1}^{N_{BS}+1} p_K(k) = 1$:

$$\begin{aligned}
\sum_k p_K(k) &= 1-(1-P_{L1})(1-P_{I1}) + \sum_{k=2}^{N}\left((1-(1-P_{Lk})(1-P_{Ik}))\prod_{j=1}^{k-1}(1-P_{Lj})(1-P_{Ij})\right) \\
&\quad + \prod_{i=1}^{N}(1-P_{Li})(1-P_{Ii}) \qquad (4.29)\\
&= 1-(1-P_{L1})(1-P_{I1}) + \sum_{k=2}^{N}\left((\prod_{j=1}^{k-1}(1-P_{Lj})(1-P_{Ij}) - \prod_{j=1}^{k}(1-P_{Lj})(1-P_{Ij}))\right) \\
&\quad + \prod_{i=1}^{N}(1-P_{Li})(1-P_{Ii}) \qquad (4.30)\\
&= 1+\sum_{k=2}^{N+1}\left(\prod_{j=1}^{k-1}(1-P_{Lj})(1-P_{Ij})\right) - \sum_{k=1}^{N}\left(\prod_{j=1}^{k}(1-P_{Lj})(1-P_{Ij})\right) \qquad (4.31)\\
&= 1+\sum_{k=2}^{N+1}\left(\prod_{j=1}^{k-1}(1-P_{Lj})(1-P_{Ij})\right) - \sum_{k=2}^{N+1}\left(\prod_{j=1}^{k-1}(1-P_{Lj})(1-P_{Ij})\right) \qquad (4.32)\\
&= 1 \qquad (4.33)
\end{aligned}$$

4.3.5 The distance between the UE and the RIS

As noticed in the equation 4.12, the expression of $\phi_{S,2}(\omega)$ depends on $d(r,l,\beta)$ and r, $d(r,l,\beta)$ being the distance between the RIS and the BS whose expression is 3.20 where beta is the angle between the link UE-RIS and UE-BS. The final expression for $\phi_{S,2}(\omega)$ is then:

$$\phi_{S,2}(\omega) = \int_{-\pi}^{\pi}\int_{r_0}^{r_{limit}} \phi_{|h_c|^2}(j(\omega P(d(r,l,\beta)+r)^{-\alpha}))f_R(r)f_\beta(\beta)\mathrm{d}r\mathrm{d}\beta \qquad (4.34)$$

where $f_R(r)$ is the pdf of the distance between the UE and the closest available RIS. As the distance between the UE and the BS is not constant, the far-field approximation from section 3.3.2 will not be used here. An available RIS satisfies the 4 criteria stated in 4.2.1. The PP of available RIS is an IPPP with density:

$$\begin{aligned}
\lambda_{RIS,av}(r) &= \frac{1}{2}\lambda_{RIS} exp\left(\frac{-2\lambda_{Obs}\mathbb{E}\left[L\right]r}{\pi}\right) exp\left(\frac{-2\lambda_{Obs}\mathbb{E}\left[L\right]d(r,l,\beta)}{\pi}\right) \\
&\quad \left(1-\frac{1}{\pi}\arccos\left(\frac{r_k - l_l cos(\beta)}{r_k^2+l_k^2-2r_k l_k cos(\beta)}\right)\right) \qquad (4.35)
\end{aligned}$$

Approximation 2

As the computation of the pdf of the distance from the closest RIS with a density of expression 4.35 would be too heavy, this PP will be simplified. An available RIS will be here defined as an RIS whose reflective side faces the UE and whose link UE-RIS is not blocked. The two other conditions stated in 4.2.1 will then be omitted. The density of this PP is now:

$$\lambda_{RIS,app}(r) = \frac{1}{2}\lambda_{RIS} exp\left(\frac{-2\lambda_{Obs}\mathbb{E}\left[L\right]r}{\pi}\right) \qquad (4.36)$$

The pdf of the distance to the closest RIS is then by first computing its cdf (or contact distribution 2.16):

$$
\begin{aligned}
F_R(r) &= 1 - exp\left(- \int_1^r \int_{-\pi}^{\pi} \frac{1}{2} \lambda_{RIS} exp\left(\frac{-2\lambda_{Obs}\mathbb{E}\left[L\right] x}{\pi} \right) x \mathrm{d}\beta \mathrm{d}x \right) && (4.37)\\
&= 1 - exp\left(-\pi \int_1^r \lambda_{RIS} exp\left(\frac{-2\lambda_{Obs}\mathbb{E}\left[L\right] x}{\pi} \right) x \mathrm{d}x \right) && (4.38)\\
&= 1 - exp\Bigg(\left[\frac{\pi}{\gamma} \lambda_{RIS} exp\left(-\gamma x\right) x \right]_1^r - \int_1^r \frac{\pi}{\gamma} \lambda_{RIS} exp\left(-\gamma x\right) \mathrm{d}x \Bigg) && (4.39)\\
&= 1 - exp\left(\frac{\pi}{\gamma} \lambda_{RIS} \Big[\left(-\gamma r + 1\right) exp\left(-\gamma r\right) - \left(\gamma + 1\right) exp\left(-\gamma\right) \Big] \right) && (4.40)
\end{aligned}
$$

where $\gamma = \frac{2\lambda_{Obs}\mathbb{E}[L]}{\pi}$.
To compute the pdf, the derivative over r must be taken:

$$
f_R(r) = -\pi\lambda_{RIS}\Big(\gamma^2(1 - F_R(r))((\gamma - \gamma^2 r)exp(-\gamma r) - \gamma exp(\gamma r) \Big) \quad (4.41)
$$

It is worth noting that as $\lambda_{RIS,app}(r) > \lambda_{RIS,av}$, the approximation will lead to an underestimation of the UE-RIS distance as there are more RIS that are available and thus, the closest RIS can be closer to the UE.
For cases where the NLoS link is important, the coverage will be overestimated by the theory compared to the simulations.

4.3.6 Coverage Probability for Different Association Rules

The previous computations are valid for the first association rule presented in subsection 4.2.2, where the UE tries to reach the closest BS either with LoS or NLoS link.
Here are the changes to apply to model the other association rules.

Removing the RIS from the network

Removing the RIS from the network can be simply modelled by setting the probability that a link going by an RIS is available to 0. Then

$$
P_{RIS}(l) = 0 \quad (4.42)
$$

Also $p_M(m)$ is then changed to:

$$
p_M(m) = \begin{cases} 1 & \text{for m=1} \\ 0 & \text{for m=2} \\ 0 & \text{for m=3} \end{cases} \quad (4.43)
$$

Prioritizing the LoS link

With this association rule, the UE will:

1. Look for a line-of-sight link for each BS from the closest to the furthest. However, if a BS can be reached with a line-of-sight link, a non line-of-sight link using a RIS will never be used.

2. If no BS can be reached with a line-of-sight link, then every BS will be checked to find a non line-of-sight link.

The theoretical changes will be on $p_K(k)$ and $p_M(m,k)$. A number of base stations reachable should be set, this can be for instance: the (rounded) average number of BS inside the disk of radius l_{limit}, then $N_{BS} = \lambda_{BS}\pi r_{limit}^2$. Here $k = 1, ..., 2N_{BS}$, if $k \leq N_{BS}$, k is the index of the BS that is reached with a LoS link. If $k > N_{BS}$, the index of the BS is $k - N_{BS}$ and can only be reached with the help of a RIS.

$$p_K(k) = \begin{cases} 1-(1-P_{L1}) & \text{if } k=1 \\ (1-(1-P_{Lk}))\prod_{i=1}^{k-1}(1-P_{Li}) & \text{if } 1<k\leq N_{BS} \\ (1-(1-P_{Ik}))\prod_{j=1}^{k-1}(1-P_{Ij})\prod_{i=1}^{N}(1-P_{Li}) & \text{if } k>N_{BS} \end{cases} \quad (4.44)$$

As the type of link used is fully determined by the index k, m stays constant when k is known. $p_M(m,k)$ then becomes:

	$k \leq N_BS$	$k > N_{BS}$
$p_M(1,k)$	1	0
$p_M(2,k)$	0	1
$p_M(3,k)$	0	0

Excluding the addition of LoS and NLoS links

In this association rule, the addition both links is excluded. If a BS can be reached using a LoS and a NLoS link, only the LoS link will be used, allowing the RIS to be used for another transmission. With this association rule, $p_M(m)$ becomes:

$$p_M(m)(P_{LOS}(l_k)+P_{RIS}(l_k)+P_{LOS}(l_k)P_{RIS}(l_k)) = \begin{cases} P_{LOS}(l_k)(1-P_{RIS}(l_k)) & \text{for m=1} \\ P_{RIS}(l_k)(1-P_{LOS}(l_k)) & \text{for m=2} \\ 0 & \text{for m=3} \end{cases} \quad (4.45)$$

4.4 Validation and results

In this section different results will be presented, those results will allow to first check the accuracy of the computation made in the previous subsection but also to compare the performances of the different association rules in different situations.
The following experiments will focus on the impact of the density of RIS λ_{RIS}, N the number of elements per RIS, the density of obstacle λ_{Obs}, the average length of an obstacles $\mathbb{E}[L]$ and the density of base station λ_{BS}.
The different experiments can be sorted in two categories: the impact of the obstacle on the coverage, increasing the density of RIS compared to increasing the density of BS.
For the following experiments, the other parameters are: $P = 10W$, $\alpha = 4$, $BW = 10MHz$, $f_c = 1.8GHz$, $r_{limit} = 600m$, $l_{limit} = 900m$ and $m = 1$.

4.4.1 Impact of blockages on the coverage probability

Several validation comments can be made about figure 4.2:

- The maximum coverage association rule gives well a better coverage than any other simulated association rule.
- On the curve of the coverage for the rule 3 referring to the definition in 4.2.2, the approximation 1 is highlighted. As the LoS link is prioritized, the accuracy of the distribution of the distance UE-BS is important in the computation of the coverage. But as stated in the approximation 1, this approximation is neither an underestimation or an overestimation which is consistent with the plot of the coverage.

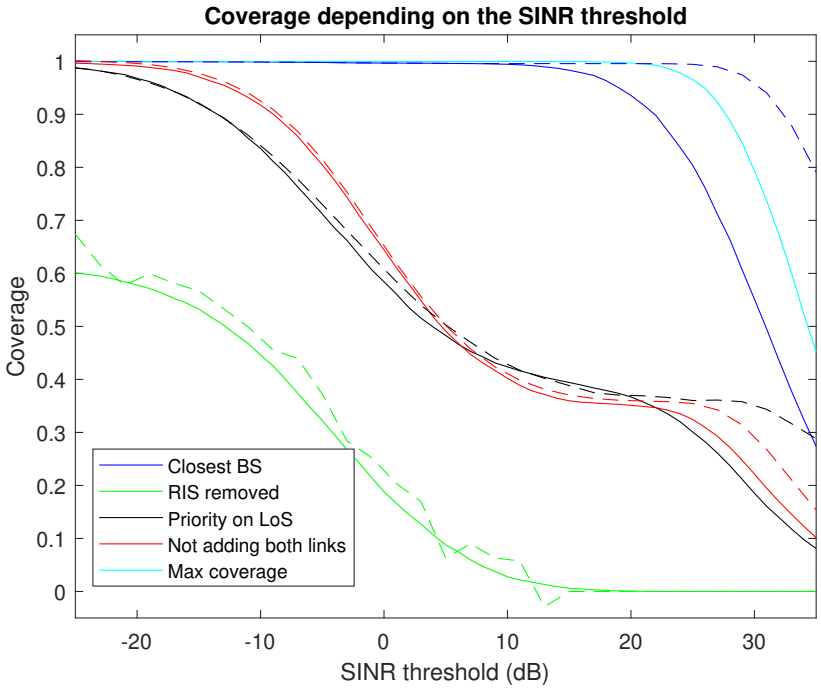

Figure 4.2: Performance of the different association rules for $\lambda_{RIS} = 800km^{-2}$, $N = 100$, $\lambda_{Obs} = 800km^{-2}$, $\mathbb{E}[L] = 15m$ and $\lambda_{BS} = 10km^{-2}$. Simulation results are in plain line, theoretical result are in dashed line

- The effect of the approximation 2 is highlighted. For rule 1 and 4, the RISs have an important impact on the establishment of the link and the coverage of rules 1 and 4 are well overestimated by the theory compared to the Monte-Carlo. Which is consistent with approximation which leads to an underestimation of the distance RIS, and thus an underestimation of the path loss impairing the NLoS link. It should also be noted that the impact of this approximation is seen for the rule 3, after $20dB$ of SINR threshold which can only be reached if a RIS is used. The coverage is there overestimated by the theory.

- For the rule 2, where the RIS are entirely removed. The theory gives follows the general results of the simulation but some peaks of error can be found. It is unlikely that they (only) come from the approximation 1 as at some point a higher SINR threshold gives a higher coverage. This error is likely due to the integration in the Gil-Pelaez inversion law which is difficult to evaluate numerically as it is unstable. As for this part the computations are heavy, only a rough estimation of the Gil-Pelaez inversion law can be done and this rough estimation seems to mainly impact the LoS link coverage probability.

When comparing the different association, it is obvious that for SINR threshold from $0dB$ to $30dB$, changing the rule of association has a very important on the performance for instance. Changing the rule 4 "Not adding both links" to rule 1 "Closest BS" increases the coverage from 75% to 100% at an SINR threshold of $0dB$. It is also worth noting that the rule 1 gives a coverage close (considering the differences between other association rules) to the one of the "maximum coverage" rule.
This set of parameters will be considered as the "base" set of parameters which will will be modified to compare the association rules in other situations.
On figure 4.3, is represented the coverage of a system where $\mathbb{E}[L]$ has been reduced to $5m$ which to probability of link being blocked very low.

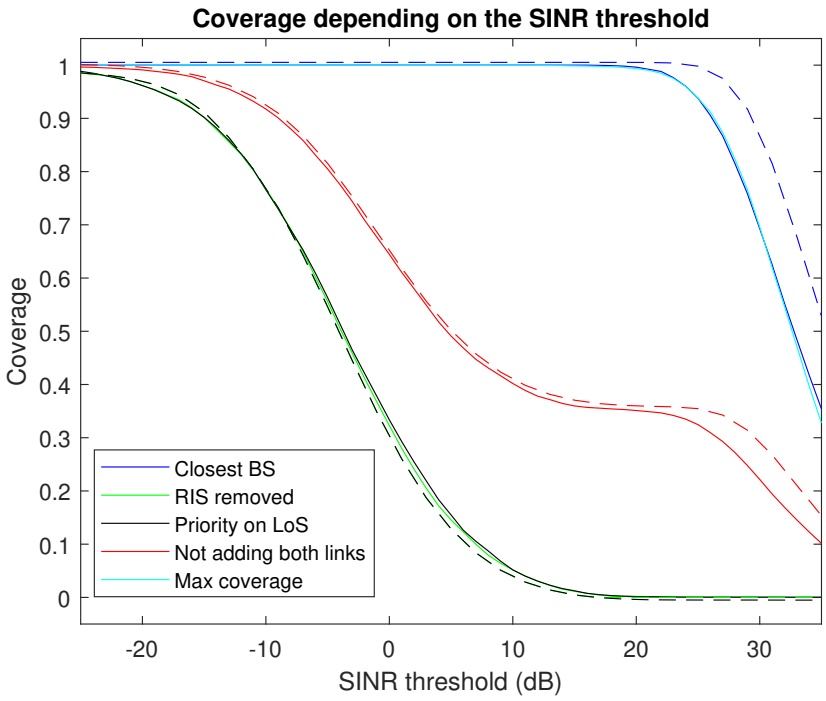

Figure 4.3: Performance of the different association rules for $\lambda_{RIS} = 800km^{-2}$, $N = 100$, $\lambda_{Obs} = 800km^{-2}$, $\mathbb{E}[L] = 5m$ and $\lambda_{BS} = 10km^{-2}$. Simulation results are in plain line, theoretical result are in dashed line

Then, the simulations and the theory matches well as the approximations 1 and 2 are mostly about the modelling of the blockages. As the blockages are unlikely, the coverage with rules 1 and 5 are close to the coverage obtained when using the closest BS and establishing both a LoS and an NLoS link. The coverage with rule 2 and 3 is close to the coverage obtained when using the first BS with a LoS link. The rule 4 leads to a better coverage than rules 2 and 3 as in the unlikely case where the LoS link to the closest BS is blocked, an RIS can be used.

4.4.2 Comparison between the density of RIS and the density of RIS

On figure 4.4 is represented a case where the blockages probability is the same as on figure 4.2, but the RIS network is less dense. The performance between the different rules of association are more similar between each other than in the 2 previous experiences. This is caused by the fact that the association rules defined here mainly act on the use of the RIS to establish a link. The difference of performance between association rules is therefore less important for a sparse network of RIS.
When comparing, the different association rules, the rule 1 is still the most efficient in terms of coverage. However the "maximum power" association rule outperforms the rule 1 by an important margin, for instance a difference of 20% of coverage for an SINR threshold of $10dB$.
On figure 4.4, the complexity of the evaluation of the Gil-Pelaez inversion law is highlighted for every theoretical model of association rule. The coverage probability should be a monotonically decreasing function depending on the SINR threshold, which is not always the case on figure 4.4, for example around $10dB$ for every association rule. As these inaccuracies appear when the used BS is likely to not be the closest BS and these inaccuracies worsen for high values of SINR threshold, it is likely that the error comes from the evaluation of the term of interference in expression as it is the only one depending on the SINR threshold and the UE-BS distance.
The complexity of the evaluation of the Gil-Pelaez inversion law is shown in appendice is C.

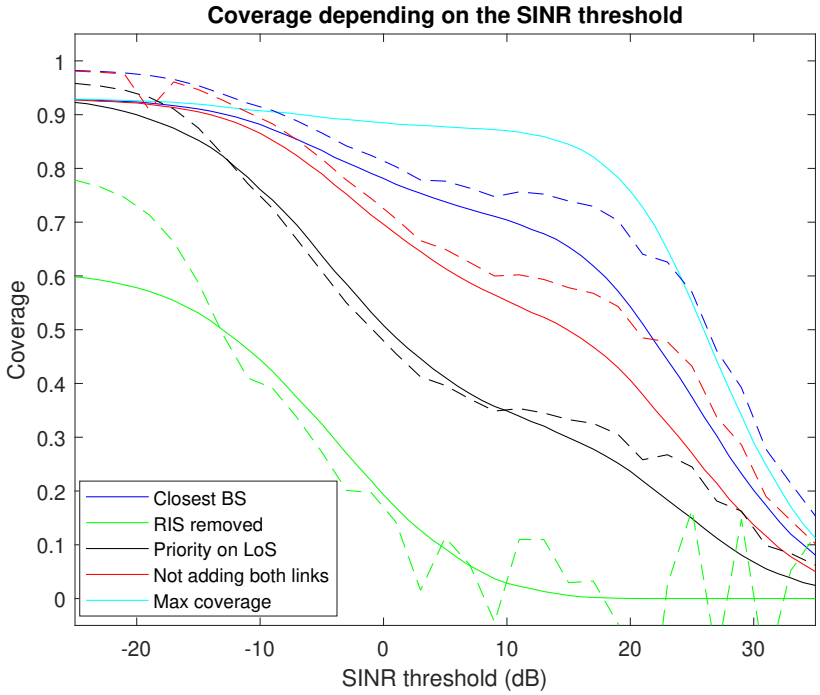

Figure 4.4: Performance of the different association rules for $\lambda_{RIS} = 100km^{-2}$, $N = 100$, $\lambda_{Obs} = 800km^{-2}$, $\mathbb{E}[L] = 15m$ and $\lambda_{BS} = 10km^{-2}$. Simulation results are in plain line, theoretical result are in dashed line

On figure 4.5, the example of a network with sparse BSs but a dense RIS network is taken. The main observation is that the 4 association rules which uses RISs gives similar performance. As the BS network is very sparse, every association rules can probably use the same BS. Then 3 "clusters" of coverage curve can be seen: the coverage when only the LoS link is used (rule 2), the coverage when only the NLoS link is used (rules 3 and 4) and the coverage when both the LoS and the NLoS link are used (rule 1 and 5).
It is worth noting that compared to figure 4.4, there is an upper bound of coverage at about 82% (in simulation) on figure 4.5 which is lower than the upper bound on figure 4.4. In the first case, there is a more dense BS network, therefore the probability that the LoS link is used is higher than in the second case where the BS network is more sparse but the RIS network is denser. The condition for a LoS link to be not blocked is less restrictive than the conditions for a NLoS link to not be blocked (see section 4.2.1). As the upper bound corresponds to the probability that the link is not blocked, the upper bound is higher with a dense BS network than with a RIS network.
On figure 4.6, each RIS has 500 elements instead of 100 in figure 4.5. The 3 "clusters" of coverage are still present. The upper bound is the same as it only depend on the geometry of the network, but for SINR threshold higher than $15dB$ the performance are getting better as the RIS of 500 elements provides a higher gain as it is more directive.

4.5 Chapter summary

Association rules comparison

In all the experiments, the association rule 1 where the closest BS reachable with a LoS and/or a NLoS link is taken was the one that provided the coverage that was the most similar to the maximum coverage.

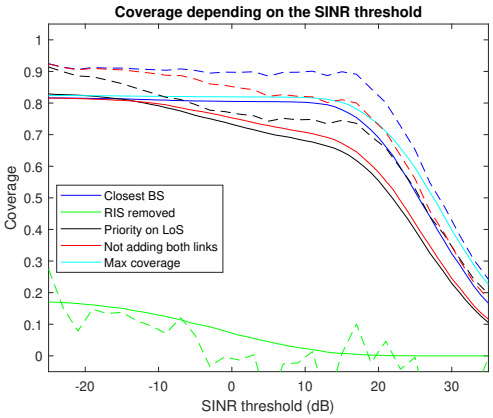

Figure 4.5: Performance of the different association rules for $\lambda_{RIS} = 800km^{-2}$, $N = 100$, $\lambda_{Obs} = 800km^{-2}$, $\mathbb{E}[L] = 15m$ and $\lambda_{BS} = 2km^{-2}$. Simulation results are in plain line, theoretical result are in dashed line

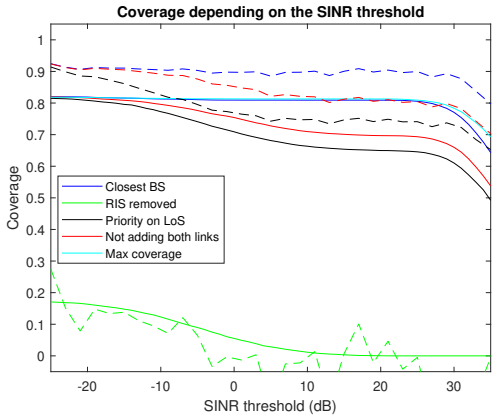

Figure 4.6: Performance of the different association rules for $\lambda_{RIS} = 800km^{-2}$, $N = 500$, $\lambda_{Obs} = 800km^{-2}$, $\mathbb{E}[L] = 15m$ and $\lambda_{BS} = 2km^{-2}$. Simulation results are in plain line, theoretical result are in dashed line

The association rule 2 where the RIS are not used has always given the worst coverage out of all the studied association rule in situations where the probability of blockage was high. In a situation with few blockages, the association rule 3 (priority on LoS link) had about the same performance as the association rule 2 but all the other association rules largely outperform them (see figure 4.3). A possible improvement on the association rule 3 would be to allow to add an NLoS link when a LoS link is available towards a BS.
The association rule 4, where the LoS and NLoS link can't be added, gives a coverage close to the maximum in situation with a low probability of blockages.

Network design

In the design of a network, 3 factors can be chosen, the density of BS, the density of RIS and the number of elements on each RIS. The advantages and drawbacks of increasing each factors are summarized in the table below:

Factor increased	Advantage	Drawback
Density of BS	Decreased probability of not having any available BS. The used BS is closer, thus receives an higher average signal power	Energy consumption Cost
Density of RIS	Energy-efficient Quality of signal improved as the RIS are made to be directive Channel Hardening	Probability of having only unavailable BS. RIS should be installed on obstacles
Number of elements	Reflection gain increased	Vulnerable to blockages

Table 4.1: Advantages and drawbacks of increasing the density of BS, the density of RIS and the number of elements of a RIS in a network.

As summarized in table 4.1, none of the options are the perfect solution and designing a robust network should use all of the three options. If performance was the only concern, then there should be a very dense BS network to ensure the best coverage possible. But using RIS should be considered in order to design a feasible network as in a real situations, energy consumption and cost are non-negligible option.

However, the effects of increasing the density of RIS or the number of elements will be limited by the fact that the RIS are installed on what is considered obstacles and by the fact that using an RIS is only possible when the incident wave and the reflected wave are not blocked.

Chapter 5

Conclusion

5.1 Summary of Contributions

In this master thesis, new stochastic geometry models have been proposed and analysed to investigate the performance of a RIS-aided wireless network.
First, a situation where the UE and the BS have known locations and where the RIS and the interfering BS are randomly located has been studied. Analytical expression have been derived to evaluate the coverage probability when multiple RIS are used coherently and where the channels are impaired by Nakagami-m distributed small scale fading. The expression for the Laplace transform of the interfering power under Nakagami-m distributed small scale fading for a finite-sized interfering BS network has also been derived. This expression have been validated by Monte-Carlo simulations under different assumptions. This provides insights on the potential of using multiple RIS to enhance the coverage.
Then, a network with multiple randomly located RIS, obstacles and BS has been modelled. Different association rules using only one RIS at a time have been defined and compared. The complexity of the evalution of the Gil-Pelaez inversion law has been highlighted. Besides the association rule which choose the BS with the maximum SNR possible, the association rule with the best coverage is to take the closest BS using both the LoS and NLoS link if possible. Finally, the results show that the optimization of the wireless network is done by in the same time having a dense network of BS with a dense network of large RIS.

5.2 Further research directions

Within the framework of this work

- In chapters 3 and 4, a more accurate propagation model form the reflection of a wave by an RIS could be used, taking in to account the real radiation pattern and the limits of configuration of the RIS.
- In chapter 3, instead of modelling by an HPPP. An IPPP could be used to model the fact that the reflective side of the RIS should face both the incident and reflected wave.
- In chapter 4, some association rules could be added or changed. For instance, allowing to use both the LoS and NLoS link when the LoS link is prioritized.
- In the computation of the interference, the interference reflected by the RIS could also be taken into account.
- Propagation model valid for mmWave communications can also be used, such as models including an absorption coefficient.

- Integrating efficient numerical evaluation of the Gil-Pelaez inversion law to improve the accuracy of the theoretical results.

Beyond the framework of this work

- In chapter 4, the assumption was taken that each possible link can be blocked independently from each others. However, in a more realistic model, there could be correlations. For instance, if two BS are very close to each other, if the LoS link from the UE to the first BS is blocked, it is likely that the LoS link from the UE to the second BS is also blocked.
- A network where RIS and unmannend aerial vehicules acting as BS has recently (May 2022) been studied [24] but not with a stochastic geometry approach. As those two technologies (RIS and UAV) are emerging technique studied for 6G wireless communications. It would be relevant to analyse a network including both RIS and UAV.

Appendices

Appendix A

Central Limit Theorem Validation

In order to use the central limit theorem to characterize $|h_c|$, it is important to compare its distribution to the real distribution (product of two Nakagami-m distributed RV) for the different numbers of elements N. When $N \to \infty$ the approximation should become more and more accurate.
Here below are the comparison of the cdf of the real distribution and the approximation of $|h_c|$ with the set of parameters $\lambda = 0.15$, $r = 50$, $d = 400$, $l = 400$, $\alpha = 4$ and $m = 0.5$.

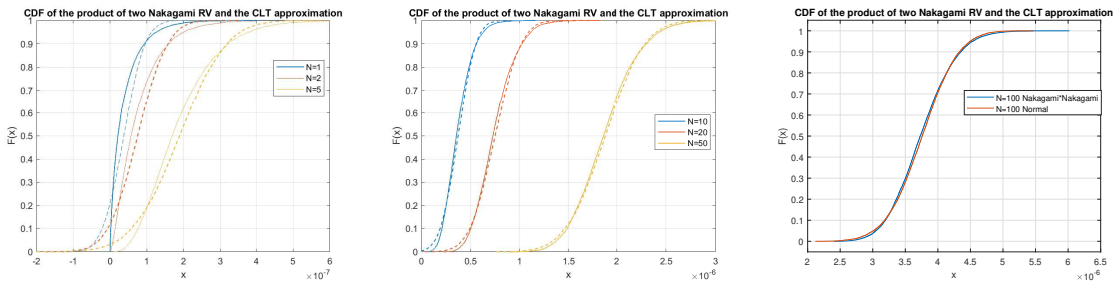

Figure A.1: CDF comparison for $m = 0.5$

On figure A.1 the real distribution is in plain line and the CLT approximation is in dashed line on the two first plots. It is obvious that when N increased, the approximation is more and more accurate. From $N = 20$ the shape of the two curves are very similar and for $N = 100$ both curves are almost superposed.
On figure A.2, the same comparison is done but for $m = 2$. And compared to $m = 0.5$ the approximation is even more accurate and from $N = 10$, the curves look superposed.
The conclusion is then that the CLT approximation becomes more accurate when N or m increases. Furthermore, in each case, the CLT approximation can be accurately used when $N > 100$.

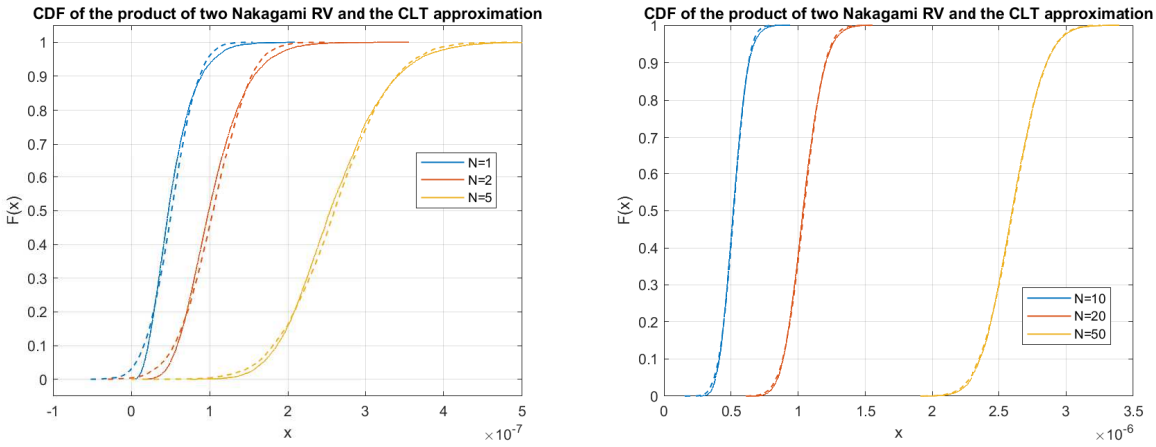

Figure A.2: CDF comparison for $m = 2$

Appendix B

Computation of the Characteristic Function of the Interfering Power

Let $I = \sum_{r_i \in \tilde{\psi}_{BS}} P\frac{\lambda^2}{16\pi^2}\varepsilon_i^2 r_i^{-\alpha}$, the Laplace transform of I is expressed by:

$$\mathcal{L}_I(s) = \mathbb{E}\left\{exp\left(-s\sum_{r_i\in\tilde{\psi}_{BS}} P\frac{\lambda}{4\pi}\varepsilon_i^2 r_i^{-\alpha}\right)\right\} \tag{B.1}$$

$$= \mathbb{E}_{\tilde{\psi}_{BS}}\left\{\prod_{r_i\in\tilde{\psi}_{BS}} \mathbb{E}_{\varepsilon_i^2}\left\{exp\left(-sP\frac{\lambda^2}{16\pi^2}\varepsilon_i^2 r_i^{-\alpha}\right)\right\}\right\} \tag{B.2}$$

Then, as $\tilde{\psi}_{BS}$ is a PPP, the PGFL of a PPP can be used:

$$\mathcal{L}_I(s) = exp\left(-\int_{\mathbb{R}^2}\left(1-\mathbb{E}_{\varepsilon^2}\left\{exp\left(-sP\frac{\lambda^2}{16\pi^2}\varepsilon^2 r^{-\alpha}\right)\right\}\right)\Lambda_{BS}(dr)\right) \tag{B.3}$$

Then given that the PPP is defined over a ring of inner radius l and outer radius l_{limit} and that the PPP has constant λ_{BS} over this region:

$$\mathcal{L}_I(s) = exp\left(-2\pi\lambda_{BS}\int_l^{l_{limit}}\left(1-\mathbb{E}_{\varepsilon^2}\left\{exp\left(-sP\frac{\lambda^2}{16\pi^2}\varepsilon^2 r^{-\alpha}\right)\right\}\right)r\mathrm{d}r\right) \tag{B.4}$$

By identifying $\mathbb{E}_{\varepsilon^2}\left\{exp\left(-sP\frac{\lambda^2}{16\pi^2}\varepsilon^2 l^{-\alpha}\right)\right\}$ as the moment generating function of ε^2 evaluated in $-sP\frac{\lambda^2}{16\pi^2}l^{-\alpha}$:

$$\mathcal{L}_I(s) = exp\left(-2\pi\lambda_{BS}\int_l^{l_{limit}}\left(1-\left(1+\frac{sP\Omega\lambda^2}{m16\pi^2 r^{-\alpha}}\right)^{-m}\right)r\mathrm{d}r\right) \tag{B.5}$$

$$= exp\left(-2\pi\lambda_{BS}\left(\frac{l_{limit}^2-l^2}{2}-\int_l^{l_{limit}}\left(1+\frac{sP\Omega\lambda^2}{m16\pi^2 r^{-\alpha}}\right)^{-m}r\mathrm{d}r\right)\right) \tag{B.6}$$

Then when working on the integral and by letting $k = \frac{sP\Omega\lambda^2}{m16\pi^2}$:

$$\int_l^{l_{limit}}\left(1+\frac{sP\Omega\lambda^2}{m16\pi^2 r^{-\alpha}}\right)^{-m}r\mathrm{d}r = \int_l^{l_{limit}}\left(1+\frac{k}{r^{-\alpha}}\right)^{-m}r\mathrm{d}r \tag{B.7}$$

$$= \int_l^{\infty}\left(1+\frac{k}{r^{-\alpha}}\right)^{-m}r\mathrm{d}r - \int_{l_{limit}}^{\infty}\left(1+\frac{k}{r^{-\alpha}}\right)^{-m}r\mathrm{d}r \tag{B.8}$$

It is then possible to show the relation between $\int_l^\infty \left(1+\frac{sk}{r^{-\alpha}}\right)^{-m} r\mathrm{d}r$ and ${}_2F_1(a,b,c;z)$ the Euler hypergeometric function:

$$\begin{aligned}
\int_l^\infty \left(1+\frac{k}{r^{-\alpha}}\right)^{-m} r\mathrm{d}r &= \int_l^\infty \left(1+\frac{k}{r^{-\alpha}}\right)^{-m} k^{1/\alpha}k^{-1/\alpha} r\mathrm{d}r && \text{(B.9)}\\
&= \int_{lk^{-1/\alpha}}^\infty \left(1+x^{-\alpha}\right)^{-m} k^{2/\alpha} x\mathrm{d}x && \text{(B.10)}\\
&= \int_{lk^{-1/\alpha}}^\infty \left(1+x^{-\alpha}\right)^{-m} k^{2/\alpha} \frac{x^{\alpha+1}k}{-\alpha l^\alpha}\frac{-\alpha l^\alpha}{x^{\alpha+1}k} x\mathrm{d}x && \text{(B.11)}\\
&= \int_1^0 \left(1+kl^{-\alpha}\right)^{-m} k^{2/\alpha} \frac{(lk^{-1/\alpha}t^{-1/\alpha})^{\alpha+1}k}{-\alpha l^\alpha} lk^{-1/\alpha}t^{-1/\alpha}\mathrm{d}t && \text{(B.12)}\\
&= \frac{-1}{\alpha}\int_0^1 \left(1+kl^{-\alpha}\right)^{-m} t^{-2/\alpha-1} l^2 \mathrm{d}t && \text{(B.13)}\\
&= {}_2F_1\left(m, \frac{-2}{\alpha}, \frac{\alpha-2}{\alpha}; -\frac{s\lambda^2 P\Omega}{16\pi^2 l^\alpha m}\right)\frac{-l^2}{2\alpha} && \text{(B.14)}
\end{aligned}$$

where B.10 is obtained by letting $x = rk^{-1/\alpha}$, B.12 is obtained by letting $t = \frac{l^\alpha}{kx^\alpha}$, the last expression is obtained by using the integral form of the Euler hypergeometric function:

$${}_2F_1(a,b,c;z) = \frac{\Gamma(c)}{\Gamma(b)\Gamma(c-b)}\int_0^1 t^{b-1}(1-t)^{c-b-1}(1-zt)^{-a} \quad \text{(B.15)}$$

Then by combining B.6, B.8 and B.14:

$$\mathcal{L}_I(s) = exp\left(\pi\lambda_{BS}\left[{}_2F_1\left(m, \frac{-2}{\alpha}, \frac{\alpha-2}{\alpha}; -\frac{s\lambda^2 P\Omega}{16\pi^2 l^\alpha m}\right) l^2 - l^2\right]_l^{l_{limit}}\right) \quad \text{(B.16)}$$

The characteristic function of I is then obtained by:

$$\begin{aligned}
\phi_I(\omega) &= \mathcal{L}_I(-j\omega) && \text{(B.17)}\\
&= exp\left\{\pi\lambda_{BS}\left[{}_2F_1(m, \frac{-2}{\alpha}, 1-\frac{-2}{\alpha}, \frac{j\omega P\Omega\lambda^2}{ml^\alpha 16\pi^2})l^2 - l^2\right]_l^{l_{limit}}\right\} && \text{(B.18)}
\end{aligned}$$

Appendix C

On the numerical evaluation of the Gil-Pelaez Inversion Law

The expression of the coverage that has to be evaluated in the second scenario is the following :

$$\mathbb{P}\left(\frac{S}{I+N_0}<\theta\right) = \frac{1}{2}-\frac{1}{\pi}\int_0^{\infty} Im\left[\left(\sum_{k=1}^{N_{BS}}\left(\int_0^{l_{limit}}\left(\sum_{m=1}^{3}\phi_{S,m}(\omega,k)p_M(m,k)\right)\phi_I(-\theta\omega)\right.\right.\right.$$
$$\left.\left.\left. f_{L_k}(l_k)\mathrm{d}l_k\right)p_K(k)\right)exp(-jN_0\theta\omega)\right]\omega^{-1}d\omega \tag{C.1}$$

Matlab has been used to evaluate this expression, but as the integral in ω is complex to evaluate because of the oscillating function $exp(-jN_0\theta\omega)$ the function "integral" could not be used as it was not time efficient enough. A trapeze rule has been used, with integration points chosen beforehand.
However, the number of integration points and the bound used in practice has a non-negligible influence on the accuracy of the analytic expression as shown below where the same expression is evaluated with difference parameters.
This shows that the results could have been even more accurate if more integration points had been used to evaluate the integration in the Gil-Pelaez inversion law. It should be noted though, that works exist on the numerical evaluation of the Gil-Pelaez inversion law such as [27].

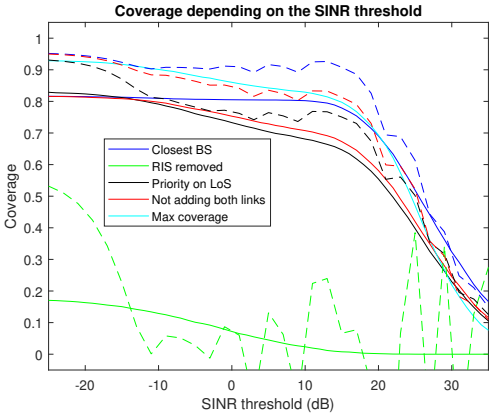

Figure C.1: Figure 4.5 when using 150 integration points from 10^{-4} to 10^{14}

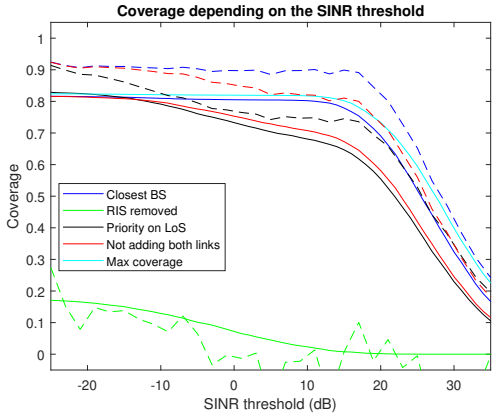

Figure C.2: Figure 4.5 when using 500 integration points from 10^{-4} to 10^{15}

Bibliography

[1] Francois Baccelli and Bartlomiej Blaszczyszyn. 2010.

[2] Tianyang Bai, Rahul Vaze, and Robert W. Heath. Analysis of blockage effects on urban cellular networks. *IEEE Transactions on Wireless Communications*, 13(9):5070–5083, 2014.

[3] Linglong Dai, Bichai Wang, Min Wang, Xue Yang, Jingbo Tan, Shuangkaisheng Bi, Shenheng Xu, Fan Yang, Zhi Chen, Marco Di Renzo, Chan-Byoung Chae, and Lajos Hanzo. Reconfigurable intelligent surface-based wireless communications: Antenna design, prototyping, and experimental results. *IEEE Access*, 8:45913–45923, 2020.

[4] Yuandan Dong, Hiroshi Toyao, and Tatsuo Itoh. Compact circularly-polarized patch antenna loaded with metamaterial structures. *IEEE Transactions on Antennas and Propagation*, 59(11):4329–4333, 2011.

[5] Hesham Elsawy, Ahmed Kamal Sultan-Salem, Mohamed-Slim Alouini, and Moe Z. Win. Modeling and analysis of cellular networks using stochastic geometry: A tutorial. *IEEE Communications Surveys & Tutorials*, 19:167–203, 2017.

[6] Gourab Ghatak, Vikrant Malik, Sanket S. Kalamkar, and Abhishek K. Gupta. Where to deploy reconfigurable intelligent surfaces in the presence of blockages? In *2021 IEEE 32nd Annual International Symposium on Personal, Indoor and Mobile Radio Communications (PIMRC)*, pages 1419–1424, 2021.

[7] Jean-Baptiste Gros, Vladislav Popov, Mikhail A. Odit, Vladimir Lenets, and Geoffroy Lerosey. A reconfigurable intelligent surface at mmwave based on a binary phase tunable metasurface. *IEEE Open Journal of the Communications Society*, 2:1055–1064, 2021.

[8] Sha Hu, Fredrik Rusek, and Ove Edfors. Beyond massive mimo: The potential of data transmission with large intelligent surfaces. *IEEE Transactions on Signal Processing*, 66(10):2746–2758, 2018.

[9] Chongwen Huang, Ronghong Mo, and Chau Yuen. Reconfigurable intelligent surface assisted multiuser miso systems exploiting deep reinforcement learning. *IEEE Journal on Selected Areas in Communications*, 38(8):1839–1850, 2020.

[10] Chongwen Huang, Alessio Zappone, George C. Alexandropoulos, Mérouane Debbah, and Chau Yuen. Reconfigurable intelligent surfaces for energy efficiency in wireless communication. *IEEE Transactions on Wireless Communications*, 18(8):4157–4170, 2019.

[11] Chongwen Huang, Alessio Zappone, Mérouane Debbah, and Chau Yuen. Achievable rate maximization by passive intelligent mirrors. In *2018 IEEE International Conference on Acoustics, Speech and Signal Processing (ICASSP)*, pages 3714–3718, 2018.

[12] Hazem Ibrahim, Hina Tabassum, and Uyen T. Nguyen. Exact coverage analysis of intelligent reflecting surfaces with nakagami-m channels. *IEEE Transactions on Vehicular Technology*, 70(1):1072–1076, 2021.

[13] Mengnan Jian, George Alexandropoulos, Ertugrul Basar, Huang Chongwen, Ruiqi Liu, Yuanwei Liu, and Chau Yuen. Reconfigurable intelligent surfaces for wireless communications: Overview of hardware designs, channel models, and estimation techniques. 03 2022.

[14] Akella S. K. Kausheek, Ashutosh Soni, T V Sreejith, and Arzad A. Kherani. Performance of ris assisted networks in noise limited and interference limited scenarios. In *2022 14th International Conference on COMmunication Systems NETworkS (COMSNETS)*, pages 565–573, 2022.

[15] Mustafa A. Kishk and Mohamed-Slim Alouini. Exploiting randomly located blockages for large-scale deployment of intelligent surfaces. *IEEE Journal on Selected Areas in Communications*, 39(4):1043–1056, 2021.

[16] Joonas Kokkoniemi and Markku Juntti. Stochastic geometry based interference analysis of multiuser mmwave networks with ris. In *2021 IEEE 32nd Annual International Symposium on Personal, Indoor and Mobile Radio Communications (PIMRC)*, pages 567–572, 2021.

[17] Sixian Li, Bin Duo, Xiaojun Yuan, Ying-Chang Liang, and Marco Di Renzo. Reconfigurable intelligent surface assisted uav communication: Joint trajectory design and passive beamforming. *IEEE Wireless Communications Letters*, 9(5):716–720, 2020.

[18] Jiangbin Lyu and Rui Zhang. Hybrid active/passive wireless network aided by intelligent reflecting surface: System modeling and performance analysis. *IEEE Transactions on Wireless Communications*, 20(11):7196–7212, 2021.

[19] Dmitri Moltchanov. Distance distributions in random networks. *Ad Hoc Networks*, 10(6):1146–1166, 2012. Publisher: Elsevier.

[20] Mahyar Nemati, Jihong Park, and Jinho Choi. Ris-assisted coverage enhancement in millimeter-wave cellular networks. *IEEE Access*, 8:188171–188185, 2020.

[21] Xilong Pei, Haifan Yin, Li Tan, Lin Cao, Zhanpeng Li, Kai Wang, Kun Zhang, and Emil Björnson. Ris-aided wireless communications: Prototyping, adaptive beamforming, and indoor/outdoor field trials. *IEEE Transactions on Communications*, 69(12):8627–8640, 2021.

[22] Marco Di Renzo, Alessio Zappone, Mérouane Debbah, Mohamed-Slim Alouini, Chau Yuen, Julien de Rosny, and Sergei A. Tretyakov. Smart radio environments empowered by reconfigurable intelligent surfaces: How it works, state of research, and the road ahead. *IEEE Journal on Selected Areas in Communications*, 38(11):2450–2525, 2020.

[23] Wankai Tang, Ming Zheng Chen, Xiangyu Chen, Jun Yan Dai, Yu Han, Marco Di Renzo, Yong Zeng, Shi Jin, Qiang Cheng, and Tie Jun Cui. Wireless communications with reconfigurable intelligent surface: Path loss modeling and experimental measurement. *IEEE Transactions on Wireless Communications*, 20(1):421–439, 2021.

[24] Kaiyuan Tian, Bin Duo, Xiaojun Yuan, and Wu Luo. Hybrid offline-online design for reconfigurable intelligent surface aided uav communication, 2022.

[25] D. Wackerly, W. Mendenhall, and R.L. Scheaffer. *Mathematical Statistics with Applications*. International student edition / Brooks-Cole. Cengage Learning, 2008.

[26] Zipeng Wang, Li Tan, Haifan Yin, Kai Wang, Xilong Pei, and David Gesbert. A received power model for reconfigurable intelligent surface and measurement-based validations. In *2021 IEEE 22nd International Workshop on Signal Processing Advances in Wireless Communications (SPAWC)*, pages 561–565, 2021.

[27] Viktor Witkovský. Numerical inversion of a characteristic function: An alternative tool to form the probability distribution of output quantity in linear measurement models. *ACTA IMEKO*, 5:32, 11 2016.

[28] He-Xiu Xu, Guang-Ming Wang, Jian-Gang Liang, Mei Qing Qi, and Xi Gao. Compact circularly polarized antennas combining meta-surfaces and strong space-filling meta-resonators. *IEEE Transactions on Antennas and Propagation*, 61(7):3442–3450, 2013.

[29] Yining Xu, Sheng Zhou, and Zhisheng Niu. The impact of interference reflection on reconfigurable intelligent surface-aided directional transmissions. In *2021 IEEE/CIC International Conference on Communications in China (ICCC)*, pages 207–212, 2021.

[30] Jia Ye, Abla Kammoun, and Mohamed-Slim Alouini. Spatially-distributed riss vs relay-assisted systems: A fair comparison. *IEEE Open Journal of the Communications Society*, 2:799–817, 2021.

[31] Özgecan Özdogan, Emil Björnson, and Erik G. Larsson. Intelligent reflecting surfaces: Physics, propagation, and pathloss modeling. *IEEE Wireless Communications Letters*, 9(5):581–585, 2020.

[32] Chao Zhang, Wenqiang Yi, Yuanwei Liu, Kun Yang, and Zhiguo Ding. Reconfigurable intelligent surfaces aided multi-cell noma networks: A stochastic geometry model. *IEEE Transactions on Communications*, 70(2):951–966, 2022.

[33] Jiayi Zhang, Hongyang Du, Qiang Sun, Bo Ai, and Derrick Wing Kwan Ng. Physical layer security enhancement with reconfigurable intelligent surface-aided networks. *IEEE Transactions on Information Forensics and Security*, 16:3480–3495, 2021.

UNIVERSITÉ CATHOLIQUE DE LOUVAIN
École polytechnique de Louvain
Rue Archimède, 1 bte L6.11.01, 1348 Louvain-la-Neuve, Belgique | **www.uclouvain.be/epl**